

The Intervening Domain Is Required For DNA-binding and Functional Identity of Plant MADS Transcription Factors

Xuelel Lai

CNRS

Rosario Vega-Leon

Humboldt-Universität zu Berlin

Veronique Hugouvieux

Commissariat à l'Énergie Atomique et aux Énergies Alternatives

Romain Blanc-Mathieu

CEA Grenoble <https://orcid.org/0000-0002-9485-6330>

Froukje van der Wal

Wageningen University and Research

Jeremy Lucas

CEA

Catarina Silva

EMBL

Agnes Jourdain

CEA

Jose Muino

Humboldt-Universität zu Berlin

Max Nanao

European Synchrotron Radiation Facility

Richard Immink

Wageningen University & Research <https://orcid.org/0000-0002-0182-4138>

Kerstin Kaufmann

Humboldt University of Berlin <https://orcid.org/0000-0001-7960-6256>

Francois Parcy

Laboratoire Physiologie Cellulaire et Végétale, Univ. Grenoble Alpes, CNRS, CEA, INRAE,

<https://orcid.org/0000-0003-2191-500X>

Cezary Smaczniak

Humboldt University of Berlin <https://orcid.org/0000-0002-4663-8275>

Chloe Zubieta (✉ chloe.zubieta@cea.fr)

CEA <https://orcid.org/0000-0003-4558-9333>

Article

Keywords: MADS transcription factors (TF), proteins, physiological roles, plant physiology

Posted Date: March 11th, 2021

DOI: <https://doi.org/10.21203/rs.3.rs-288619/v1>

License:  This work is licensed under a Creative Commons Attribution 4.0 International License.

[Read Full License](#)

Version of Record: A version of this preprint was published at Nature Communications on August 6th, 2021. See the published version at <https://doi.org/10.1038/s41467-021-24978-w>.

1 The Intervening Domain Is Required For DNA-binding and Functional Identity of Plant 2 MADS Transcription Factors

3
4 Xuelei Lai^{1,*}, Rosario Vega-Leon^{2,*}, Veronique Hugouvieux^{1,*,#}, Romain Blanc-Mathieu¹,
5 Froukje van der Wal³, Jérémy Lucas¹, Catarina S. Silva^{1,4}, Agnès Jourdain¹, Jose Muino⁵,
6 Max H. Nanao⁶, Richard Immink^{3,7}, Kerstin Kaufmann², François Parcy¹, Cezary
7 Smaczniak^{2,#}, Chloe Zubieta¹
8

9 ¹ Laboratoire Physiologie Cellulaire et Végétale, Univ. Grenoble Alpes, CNRS, CEA, INRAE, IRIG-DBSCI-
10 LPCV, 17 avenue des martyrs, F-38054, Grenoble, France.

11 ² Plant Cell and Molecular Biology, Humboldt-Universität zu Berlin, Institute of Biology, Berlin, Germany.

12 ³ Bioscience, Wageningen Plant Research, Wageningen University and Research, 6708 PB, Wageningen, The
13 Netherlands.

14 ⁴ European Molecular Biology Laboratory, Grenoble, France

15 ⁵ Systems Biology of Gene Regulation, Humboldt-Universität zu Berlin, Institute of Biology, Berlin, Germany.

16 ⁶ European Synchrotron Radiation Facility, Structural Biology Group, Grenoble, France

17 ⁷ Laboratory of Molecular Biology, Wageningen University and Research, 6708 PB, Wageningen, The
18 Netherlands.

19
20 *first

21 #correspondence
22

23 **Abstract**

24 The MADS transcription factors (TF) are an ancient protein family with a high degree of
25 sequence identity that bind almost identical DNA sequences across all eukaryotic kingdoms
26 of life, yet fulfill dramatically different physiological roles. In plants, the family is divided
27 into two main lineages, type I and II, based on sequence conservation of the DNA-binding
28 MADS-box domain (M domain) with yeast and animal M domains. Here, we demonstrate
29 that DNA binding in both lineages absolutely requires a short amino acid sequence C-terminal
30 to the M domain called the Intervening domain (I domain) in type II MADS. Structural
31 elucidation of the MI domains from the floral regulator, SEPALLATA3 (SEP3), shows a
32 highly conserved MADS-box fold with the I domain forming an alpha helix and acting to
33 stabilize the M domain. Based on secondary structure prediction, sequences fulfilling the
34 same function as the SEP3 I domain can be found in both lineages of plant MADS TFs,
35 suggesting the I domain is a conserved and required part of the DNA-binding domain. Using
36 the floral organ identity MADS TFs, SEP3, APETALA1 (AP1) and AGAMOUS (AG),
37 domain swapping demonstrate that the I domain alters DNA-binding specificity based on seq-
38 DAP-seq experiments. Yeast 2-hybrid experiments further revealed the role of the I domain in
39 dimerization specificity. Surprisingly, introducing AG carrying the I domain of AP1 in the
40 Arabidopsis *apl* mutant, resulted in a high degree of complementation and restoration of first
41 and second whorl organs. Taken together, these data demonstrate that the I domain acts both
42 as an integral part of the DNA-binding domain and strongly contributes to the functional
43 identity of the MADS TF.
44

45 **Introduction**

46 The MADS-box genes, named after founding members *MINICHROMOSOME*
47 *MAINTENANCE1* (*MCM1*, *Saccharomyces cerevisiae*), *AGAMOUS* (*Arabidopsis thaliana*),

48 *DEFICIENS* (*Antirrhinum majus*), and *SERUM RESPONSE FACTOR* (*SRF*, *Homo sapiens*),
49 is an ancient gene family present before the ancestral split of animals, plants and fungi¹⁻⁴.
50 Prior to the divergence of eukaryotes into different kingdoms of life, the MADS gene family
51 underwent a duplication event giving rise to two main lineages, the SRF-like and MEF2-like
52 lineages, which correspond to the type I and II MADS genes in plants, respectively^{6,7}. While
53 these two MADS lineages both encode a highly conserved ~60 amino acid MADS-box DNA-
54 binding domain (DBD) that recognizes a CArG box motif (CC-“Adenine rich”-GG), DNA-
55 binding preferences are slightly altered due to amino acid changes in the MADS-box domain
56 specific to each lineage⁸⁻¹¹. In addition to changes in amino acids important for direct base
57 readout, the region C-terminally adjacent to the MADS-box domain varies based on sequence
58 alignments and available structural data for mammalian and fungal SRF-like and MEF2-like
59 MADS TFs. These carboxyl terminal sequences have been shown to be important for
60 dimerization and DNA binding although they do not directly contact the DNA^{4,8,12}. While the
61 MADS genes are ubiquitous in extant eukaryotes, they have undergone a significant
62 expansion in plants, with angiosperms possessing tens of type I SRF-like and type II MEF2-
63 like MADS genes that fulfill diverse physiological roles.

64 The plant type I MADS genes generally consist of one or two exons and encode
65 transcription factors (TFs) comprised of the MADS-box DBD and a variable C-terminal
66 domain. The type I genes are further subdivided into three subfamilies, M α , M β and M γ , with
67 preferential interactions between subfamilies forming heterodimeric complexes^{13,14}. While
68 generally expressed at very low levels in a tissue specific manner, the type I genes have been
69 shown to be important in plant reproduction and speciation, with crucial roles in female
70 gametophyte, embryo, and endosperm development^{15,16}. In contrast to the simple one or two
71 exon composition and protein structure of the type I MADS, the type II genes consist of 5-8
72 exons and encode TFs with a modular four-domain structure, called “MIKC”¹⁷⁻¹⁹. The MIKC
73 domains refer to M, for MADS DBD, I for the dimerization specifying Intervening domain, K
74 for the coiled-coil keratin-like domain involved in dimer and tetramer formation and C for the
75 variable C-terminal domain important for transactivation and higher order complex formation.
76 The type II MADS are further subdivided into the MIKC* and MIKC^C subfamilies based on
77 the structure of the I domain, with dimerization mainly occurring within the same subfamily,
78 but not between subfamilies²⁰⁻²². While all MADS TFs are believed to form dimeric
79 complexes in order to bind DNA, the type II MADS TFs are able to tetramerise via the K
80 domain, greatly expanding the number of possible MADS complexes that can be formed²³⁻²⁵.
81 The diversity of heteromeric complexes the type II MADS form is hypothesized to be directly

82 tied to their functional diversity²⁶. The type II MADS play well established roles in many
83 developmental processes including meristem identity, flowering time, fruit and seed
84 development and floral organ identity²⁷.

85 The MADS TFs involved in floral organ specification are arguably the most well
86 studied MADS family members and provide an ideal model to examine function *in planta*.
87 Elegant *in vitro* and *in vivo* experiments dating back decades have tried to address the
88 question of how plant MADS TF achieve their DNA-binding specificity and functional
89 diversity in the context of flower and floral organ development^{28,29}. Four classes of MIKC
90 MADS TFs, class A, B, C and E are necessary for floral organ identity. The A+E class
91 specify sepals, the A+B+E petals, A+C stamen and C+E carpels. In Arabidopsis, these
92 correspond to APETALA1 (AP1, A class), APETALA3 (AP3, B class) and PISTILLATA
93 (PI, B class), AGAMOUS (AG, C class) and the four SEPALLATAs (SEP1 -4, E class). The
94 generation of chimeric MADS TFs with swapped M domains from AP1, AP3, PI and AG
95 demonstrated that the MADS domains of these proteins were interchangeable with respect to
96 their *in vivo* function^{29,30}. Even swapping in portions of human or yeast M domains, which did
97 alter *in vitro* DNA-binding, did not alter the function of the MADS proteins *in vivo*,
98 suggesting that the physiological function of these proteins seems to be independent of the
99 DNA-binding domain³⁰. Thus, tetramerisation in MIKC MADS TFs came under scrutiny as a
100 potential determinant of DNA-binding syntax by selecting for two-site DNA-binding
101 constrained by specific intersite distances^{31,32}. More recent studies of a tetramerisation mutant
102 of SEP3 revealed that while tetramerisation contributed to *in vivo* function, *in vitro* changes in
103 DNA-binding specificity genome-wide were more limited, putatively affecting a relatively
104 small number of key gene targets whose regulation depends on specific spacings between
105 CArG box binding sites^{32,33}. Thus, the fundamental question of how plant MADS TFs are able
106 to recognize different DNA sequences critical for the regulation of different target genes, with
107 apparently interchangeable DBDs, is still not fully resolved.

108 In order to address this, we performed structural, biochemical, genome-wide binding
109 and *in vivo* studies focusing on the role of the Intervening domain. We demonstrate that an I-
110 like domain is present in both type I and type II plant MADS TFs and that this region is
111 required for DNA-binding, affects DNA-binding specificity and alters dimerization specificity
112 *in vitro* and in yeast assays. Seq-DAP-seq experiments comparing SEP3-AG and SEP3-
113 AG^{IAP1}, a chimera with the I domain from AG replaced by the I domain of AP1, revealed
114 unique binding sites for each complex, changes in preferred site spacing and a loss of carpel
115 and fourth whorl-specific targets for the chimeric protein. Using these same floral organ

116 identity MADS TFs to probe *in vivo* function of the I domain, different chimeric constructs
117 were introduced into the *ap1* background. Interestingly, replacing the I domain of *AG* with
118 that of *API* was sufficient to confer the majority of *API* functions *in planta* including sepal
119 and petal identity in the first and second whorls. Taken together, these data illustrate the
120 importance and multiple roles of the I domain in DNA-binding and *in planta* function.

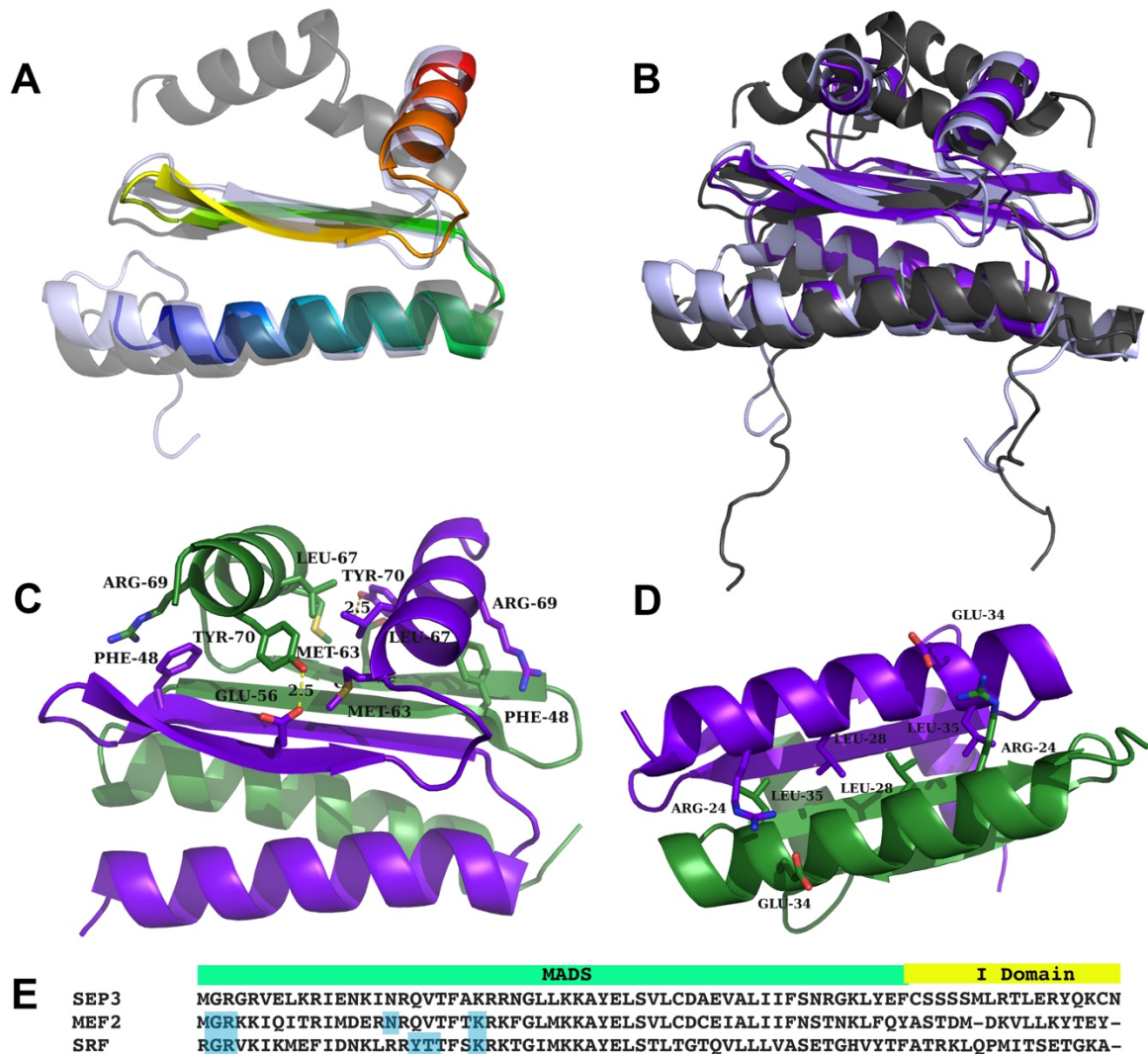
121

122 **Results**

123 **Structure of the SEPALLATA3 MI domain**

124 The MADS-box and I domain of SEP3 (SEP3^{MI}, residues 1-90) was used in structural
125 studies as this construct has been shown to be dimeric in solution and to bind DNA in a
126 sequence specific manner³⁴. SEP3^{MI} crystallized in spacegroup C222₁ with 4 monomers per
127 asymmetric unit and diffraction to 2.1 Å (**Table 1**). The first 18 amino acids, which are
128 predicted to have no defined secondary structure, were disordered as were the 17 C-terminal
129 amino acids, and no electron density was interpretable for these portions of the protein in any
130 of the molecules. Each monomer adopts the same tertiary structure with an N-terminal alpha
131 helix (α 1; aa 18-40) and two antiparallel beta strands (β 1; aa 44-48 and β 2; aa 55-58). These
132 elements make up the core MADS DBD and are conserved in the MEF2 and SRF-like MADS
133 TFs (**Figure 1A and B**). C-terminal to the beta strands is a short loop followed by an alpha
134 helix which is contributed by the I domain (α 2; aa 63-73). The orientation of the C-terminal
135 alpha helix differs between MEF2 (PDB codes 1EGW, 1C7U, 1TQE, 3KOV) and SRF-like
136 MADS TFs (PDB code 1HBX), with SEP3^{MI} resembling the MEF2 structure. Overall,
137 SEP3^{MI} adopts the MADS/MEF2 fold, as predicted for type II plant MADS TFs.

138 Each SEP3^{MI} monomer dimerizes via extensive contacts between the pairs of alpha
139 helices and beta strands from each partner, with dimerization required for DNA binding. In
140 the structure, all dimers were formed by crystallographic symmetry, with dimerization
141 burying over 25% of the total surface area of the molecule (**Figure 1**)³⁵. The dimer interface
142 includes hydrophobic interactions between residues in the N-terminal DNA-binding alpha
143 helices, Leu28 and Leu35, and pairs of salt bridges between Glu34 and Arg24 (**Figure 1D**).
144 The formation of a 4-stranded antiparallel beta sheet further stabilizes the quaternary structure
145 of SEP3 with interactions bridging the N-terminal DNA binding helices and the C-terminal I
146 domain helices. The I domain helices sandwich the beta sheet and lie perpendicular to the
147 DNA-binding helices of the MADS-box domain. The I domain is anchored to the beta sheet
148 via hydrogen bonding interactions between Glu56 and Tyr70 and pi-cation interactions
149 between Phe48 and Arg69 of the partner monomers. Each I domain helix also interacts with



150
151
152
153
154
155
156
157
158
159

Figure 1. Structure and sequence of the SEP3 MI domain and corresponding SRF and MEF2 regions. (A) Overlay of SEP3 dimer (rainbow) and SRF (1HBX) dimer (gray). The I region is alpha helical for both structures, however the contacts with the M domain differ. (B) Overlay of SEP3 (dark purple) and MEF2A (3KOV, light purple) and SRF (gray) demonstrating the different conformations of the I region in the type II (MEF2-like) and I (SRF-like) MADS TFs. (C) SEP3 dimer with one monomer in purple and one in green. Amino acids important for interactions between I domains and between M and I domains are labelled and drawn as sticks. Hydrogen bonds are shown as dashed yellow lines. (D) View of the I domain with intermolecular interactions from the N-terminal alpha helices shown. (E) Partial sequence alignment of SEP3 (accession NP564214.2), MEF2 (accession AAB25838.1) and SRF (accession P11831) corresponding to the region in the crystal structure. Residues directly contacting the DNA for MEF2 and SRF are highlighted in blue.

160 its dimer partner helix via hydrophobic interactions mediated by Leu67, Tyr70 and Met63
161 (**Figure 1C**). These residues are highly conserved in all MIKC MADS TFs from Arabidopsis,
162 suggesting that the interactions are also conserved and likely important for structural stability
163 of plant MADS TFs. Mutations R69L (present in APETALA3), R69P (present in
164 FLOWERING LOCUS M-delta) and Y70E (present in FLM-delta) destabilized SEP3^{MI} based
165 on thermal shift assays, as predicted from the structural data (**Supplementary Figure 1**).

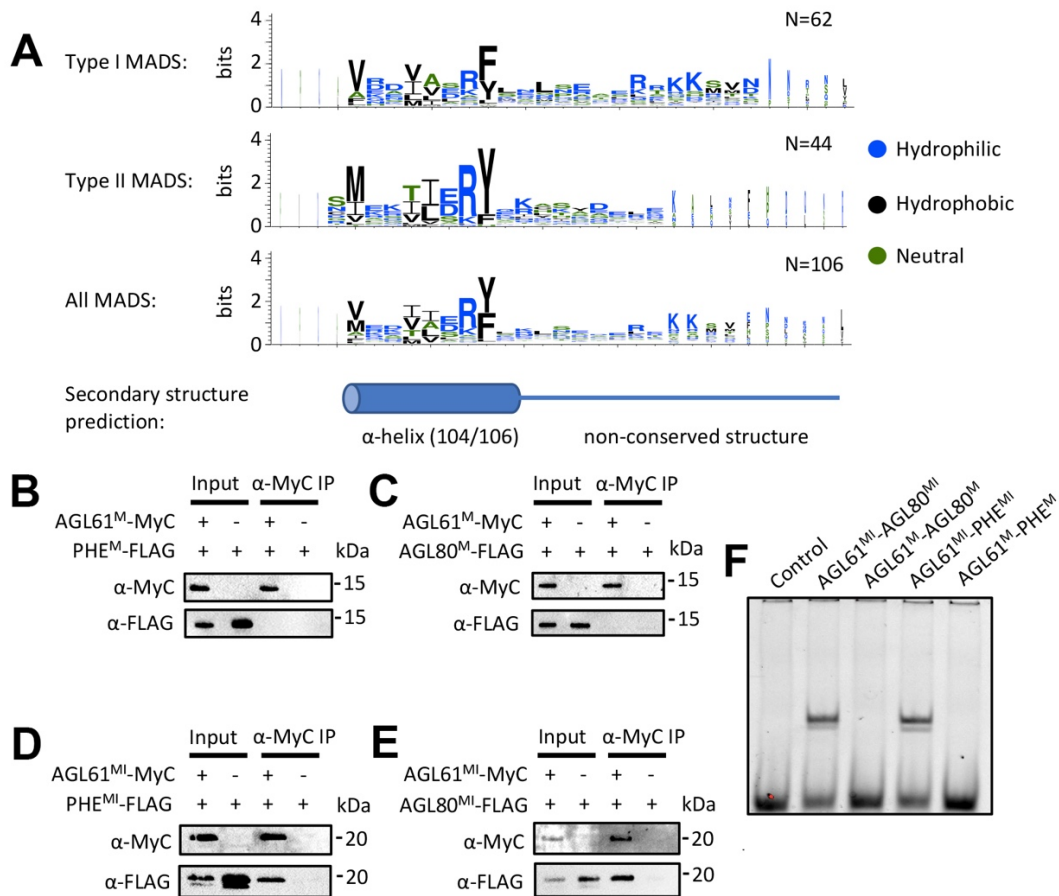
166 SEP3^{MI} was crystallised without DNA, however, multiple DNA-bound structures of
167 the closely related MEF2 protein are available for comparison. Structural alignment of
168 SEP3^{MI} with the corresponding MEF2 structure reveals a rmsd of 0.942 Å², underscoring the

169 conservation in the MADS/MEF2 domains with the MADS/I domains of SEP3^{MII} (**Figure 1A,**
170 **B**). The residues directly contacting the DNA are contributed from the flexible N-terminus
171 and the N-terminal helix of the MADS-box domain, with no direct contacts from the MEF2/I
172 domain (**Figure 1E**). These DNA-binding residues are highly conserved in SEP3 even though
173 MEF2 recognizes a YTA(A/T)₄TAR sequence (Y=pyrimidine, R=purine), whereas SEP3
174 recognizes a classic CArG box motif (CC(A/T)₆GG). The differences in DNA-binding
175 specificity of the MEF2-like MADS TFs coupled with the high conservation of sequence and
176 structure of the MADS-box domain itself, suggest allosteric contributions from the MEF2/I
177 domain may play a role in DNA binding. Indeed, examining the DNA-binding of the I
178 domain mutants R69L, R69P and Y70E demonstrated that these single point mutations were
179 sufficient to abrogate the DNA binding activity of the full-length SEP3 based on
180 electrophoretic mobility shift assays (EMSAs) (**Supplementary Figure 1**).

181

182 **Type I and II MADS possess I-like domain sequences required for DNA-binding**

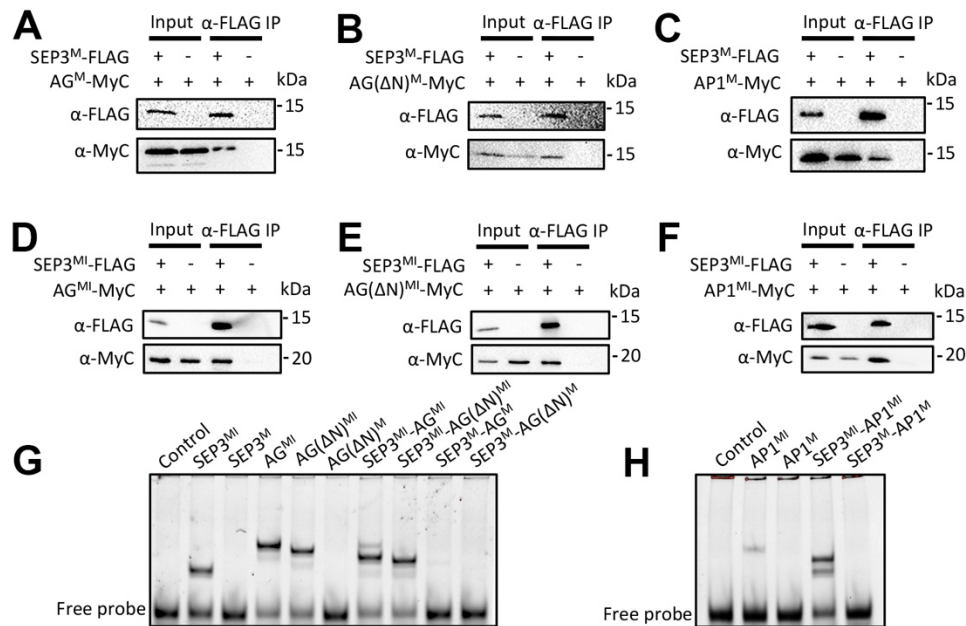
183 Structural and mutagenesis data suggest that the MEF2/I domain is critical for stability
184 and DNA-binding of type II MADS TFs. The type I plant MADS TFs do not possess an I or
185 MEF2-domain and are more closely related to the SRF-type MADS TFs. However, the
186 structure of SRF (PDB 1HBX) reveals a similar alpha helical region C-terminal to the
187 MADS-box domain, albeit with a different orientation of helices from the MEF2/I domain
188 (**Figure 1A**). Protein sequence alignment of the 106 MADS TFs from Arabidopsis reveal that
189 104 of the 106 sequences possess ~15 amino acids C-terminal to the MADS domain that are
190 structurally conserved and predicted to form alpha helices with similar physicochemical
191 properties (**Figure 2A**). In particular, positions including Arg69 and Tyr70 in SEP3 that are
192 important for I domain anchoring to the M domain are conserved in both type I and type II
193 MADS, while a high degree of sequence variation in the non-alpha helical region is observed
194 (**Figure 2A and Supplementary Figure 2**). This suggests that these ~15 amino acids in type
195 I MADS TFs may act as an I-like alpha helical domain and stabilize the structure of the DBD,
196 influence DNA-binding specificity or both.



197
 198 **Figure 2. Type I MADS possesses I domain like region which is required for both dimerization and DNA binding.** (A)
 199 Amino acid enrichment of the I region (~30 amino acids C-terminal to the M domain) of type I, type II and all MADS TFs,
 200 logos generated with WebLogo³⁶. The overall height of the stack in each position indicates the sequence information content
 201 at that position, while the height of the amino acid symbols within the stack indicates the relative frequency at each position.
 202 The MADS TF sequences are taken from The Arabidopsis Information Resource (www.arabidopsis.org). (B-C) Pull-down
 203 assay showing that M domain of AGL61 (AGL61^M) does not interact with the M domain of PHE (PHE^M) or AGL80
 204 (AGL80^M). (D-E) Pull-down assay showing that the M domain plus the I like region of AGL61 (AGL61^{MI}) interacts with the
 205 MI region of PHE (PHE^{MI}) and AGL80 (AGL80^{MI}). (F) EMSA assay showing that heterodimers AGL61^{MI}-AGL80^{MI} and
 206 AGL61^{MI}-PHE^{MI} shift a DNA sequence containing a canonical CARG-box binding site from the *SEP3* promoter, while their
 207 corresponding constructs without the I region do not exhibit any binding.
 208

209 To further determine the role of the alpha helical region adjacent to the M domain in
 210 both type I and II MADS (called for simplicity the I region hereafter), we performed pull
 211 down experiments and EMSAs for representative MADS TFs from Arabidopsis. We chose
 212 AGAMOUS-LIKE 61 (AGL61) from subclass M α and AGAMOUS-LIKE 80 (AGL80) and
 213 PHERES1 (PHE1) from subclass M γ for type I MADS TFs, as interaction patterns of these
 214 have been previously studied^{37,38}. Pull-down experiments revealed that the M+I region of
 215 AGL61 (AGL61^{MI}) interacts with the M+I region of AGL80 (AGL80^{MI}) or PHE1 (PHE1^{MI}),
 216 while the M domains alone are not sufficient for interaction (**Figure 2B-E**), suggesting that
 217 the I region in type I MADS TFs is required for stable dimerization. Consistent with this,

218 EMSAs show that while heterodimers of AGL61^{MI}-AGL80^{MI} and AGL61^{MI}-PHE1^{MI} bind to a
 219 canonical CArG box motif, the M domains alone exhibit no DNA binding (**Figure 2F**).



220
 221
 222
 223
 224
 225
 226
 227

Figure 3. Type II MADS TFs require the I domain for DNA binding but not dimerization. (A-C) Pull-down assay showing that the M domain of SEP3 (SEP3^M) interacts with the M domains of AG (AG^M), AG with the first 16 N-terminal amino acids deleted (AG(ΔN)^M) and AP1 (AP1^M), respectively. (D-F) Pull-down assay showing that the MI domain of SEP3 (SEP3^{MI}) interacts with the MI domain of AG^{MI}, AG(ΔN)^{MI} and AP1^{MI}, respectively. (G and H) EMSA assay showing that homodimers from SEP3^{MI}, AG^{MI}, AG(ΔN)^{MI} and AP1^{MI}, and heterodimers SEP3^{MI}-AG^{MI}, SEP3^{MI}-AG(ΔN)^{MI} and SEP3^{MI}-AP1^{MI} shift a DNA sequence containing a canonical CArG-box binding site (as per Figure 2), while their corresponding constructs without the I domain can not, suggesting that the I domain in type II MADS TFs is required for DNA binding.

228 For the type II MADS TFs, we generated M domain and MI domain constructs for
 229 SEP3, AP1 and AG. In Arabidopsis, SEP3-AP1 containing MADS TF complexes define first
 230 and second whorl flower organs (sepal and petals) whereas SEP3-AG containing complexes
 231 are required for third and fourth whorl (stamen and carpel) flower organ identity. We focused
 232 on these MADS TFs as their heterocomplex formation, DNA-binding specificity and *in vivo*
 233 activity are well understood^{11,14,23,39-43}. As expected, the MI domain of SEP3 interacts with
 234 that of AP1 and AG (**Figure 3D-F**). However, in contrast to the type I MADS, the M domain
 235 of SEP3 is able to pull down the M domains of AP1 and AG (**Figure 3A and C**). As AG
 236 possesses an N-terminal 16 amino acid extension, constructs with and without these amino
 237 acids were tested. Both constructs were able to interact with the M domain of SEP3 (**Figure**
 238 **3A and B**). Thus, unlike the type I MADS TFs tested, the M domain alone of the type II
 239 MADS TFs tested was sufficient for protein-protein interaction. However, the M domains
 240 alone of SEP3-AP1 and SEP3-AG were unable to bind a canonical CArG DNA motif in
 241 EMSA experiments (**Figure 3G and H**), suggesting that the M domain of type II without the
 242 I domain is not sufficient to form a stable dimer for DNA binding. In contrast, homo and

243 heterodimers of the MI domains of SEP3, SEP3-AP1, AP1, AG and SEP3-AG were all able
244 to bind DNA under our experimental conditions (**Figure 3G and H**). Taken together, these
245 data suggest that the I domain, while possessing no direct interactions with DNA, is essential
246 for DNA-binding for both type I and type II MADS TFs, likely by stabilizing the MADS TF
247 dimer.

248 **Impact of the I domain on DNA-binding specificity and intersite spacing**

250 To further explore the role of the I domain in DNA-binding specificity, we focused on
251 the floral organ identity-specifying MADS TFs, SEP3, AP1, AG and a chimeric version of
252 AG, in which the AG I-domain was replaced with the AP1 I-domain (AG^{IAP1}). Using
253 sequential DNA-affinity purification followed by sequencing (seq-DAP-seq ref), we
254 determined the DNA-binding of the heteromeric complexes of SEP3-AG³² and SEP3-AG^{IAP1}
255 (this study). Unfortunately, the SEP3-AP1 heteromeric complex under the same experimental
256 conditions did not yield data of sufficient quality for analysis. However, SEP3-AG and SEP3-
257 AG^{IAP1} strongly bound DNA and each produced highly similar replicates for data analysis
258 (**Supplementary Fig. 3**). We used a highly stringent peak calling for each replicate and peaks
259 were kept only when present in all replicates. This yielded 6,347 peaks for SEP3-AG and
260 3,552 peaks for SEP3-AG^{IAP1}. These peak lists were merged and the binding intensities for
261 the two complexes were compared for all resulting peaks. This profiling indicates that while
262 most peaks have a similar binding intensity, several hundred exhibited at least a two-fold
263 difference in binding intensity between SEP3-AG and SEP3-AG^{IAP1} (**Figure 4A-B**). The same
264 profiling between replicates for a given dataset demonstrated no such variability in binding
265 intensity (**Supplementary Figure 3**).

266 The top 15% sequences (1,073 sequences for each complex) displaying the most
267 extreme binding difference were used to search for specific DNA patterns that potentially
268 code for SEP3-AG and SEP3-AG^{IAP1} differential response. The TF binding sites were
269 modeled using position weight matrices, transcription factor flexible models and k-mer set
270 memory (KSM) analysis. Due to the highly similar binding modes of the MADS family TFs,
271 only KSM was sensitive enough to differentiate the MADS heterocomplexes (**Figure 4C and**
272 **D**)⁴⁴. For the KSM, pipeline, KMAC and KSM tools from the GEM package⁴⁵ were used to
273 search for clusters of short (4-20 bp) overlapping sequences (with allowances and penalties
274 for gaps and mismatches) that are over-represented in the top 15% of SEP3-AG and SEP3-
275 AG^{IAP1} specific bound sequences. This analysis yielded 55 clusters for SEP3-AG and 22
276 clusters for SEP3-AG^{IAP1} and served as kmer-based models for prediction analysis. With

277 AUC of 0.79 for SEP3-AG and 0.84 for SEP3-AG^{IAP1}, the kmer-based models were highly
278 predictive. Importantly, each kmer-based model did not perform well (AUC ~0.7) in
279 predicting bound regions from the other heterocomplex (**Figure 4D**). This suggests that
280 specific sequence patterns code for differential binding between the two heterocomplexes.

281 Previously, using seq-DAP-seq, we showed that SEP3-AG demonstrates preferential
282 intersite spacing of ~47 and ~57 bp between two CARG boxes due to its cooperative binding,
283 a contributing factor for DNA-binding specificity of MADS TF complexes³². Using specific
284 bound regions of SEP3-AG^{IAP1} when compared with SEP3-AG, we found that SEP3-AG^{IAP1}
285 gained new preferential intersite spacings of 25 and 34 bp and lost the SEP3-AG preferential
286 intersite spacings (**Figure 4E**). This further suggests that the I domain plays a role in DNA-
287 binding specificity by affecting the conformation of the tetramer and selecting for specific
288 intersite distances.

289 In order to determine whether these observed *in vitro* differences in binding were
290 potentially relevant *in vivo*, we examined published ChIP-seq datasets. Previous studies have
291 shown that the *in vitro* binding of SEP3-AG relative to SEP3-AP1 in SELEX-seq correlates
292 with the *in vivo* binding intensity of AG relative to AP1 in ChIP-seq for the 1500 most
293 enriched SEP3 ChIP-seq peaks (**Figure 4F**)⁴⁴. This result suggested that specific sequence
294 patterns detected *in vitro* were able to at least weakly discriminate sequences either more
295 likely to be bound by SEP3-AG or by SEP3-AP1 in the Arabidopsis genome. Applying the
296 same analysis to our seq-DAP-seq data, we found a similar weak positive correlation between
297 the SEP3-AG binding affinity relative to that of SEP3-AG^{IAP1} and the corresponding ChIP-
298 seq derived *in vivo* binding, suggesting that SEP3-AG^{IAP1} behaves more similarly to SEP3-
299 AP1 than to SEP3-AG (**Figure 4F**). Although modest, this correlation is supported by the
300 observation that the genes corresponding to the 250 peaks most differentially bound by SEP3-
301 AG relative to SEP3-AG^{IAP1} exhibited a 7.6-fold enrichment for genes involved in “carpel
302 development” GO term (FDR = 4.2 x 10⁻³). However, no clear GO term enrichment was
303 detected for genes corresponding to the 250 regions best bound by SEP3-AG^{IAP1} relative to
304 SEP3-AG. This may be due to the relatively small number of genes corresponding to GO
305 terms for “petal development” (4 genes) and “sepal development” (13 genes), suggesting an
306 incomplete list of genes for these GO terms. Taken together, the binding differences between
307 the SEP3-AG^{IAP1} and SEP3-AG complex suggest that the AG^{IAP1} protein has lost some AG
308 identity and gained AP1-like identity.

309

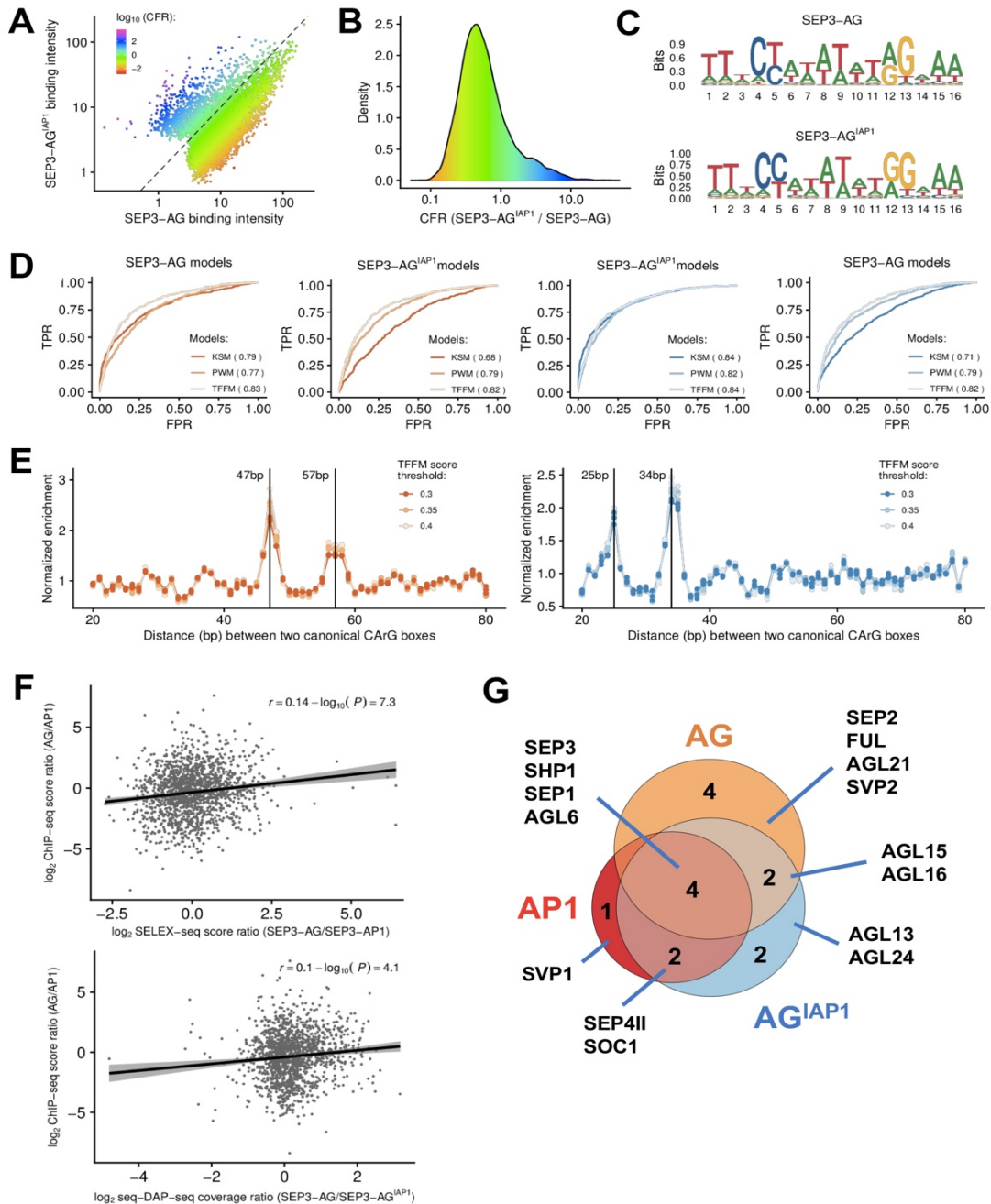


Figure 4. DNA-binding and protein interactions patterns. (A) Comparison of SEP3-AG and SEP3-AG^{IAP1} seq-DAP-seq binding intensity (log₁₀ of reads per kb per million of reads mapped in bound regions) and color-coded by purple-blue (SEP3-AG^{IAP1}-specific) to orange-red (SEP3-AG-specific) according to log₁₀ of SEP3-AG^{IAP1}/SEP3-AG. (B) Density plot showing data as per A. (C) Logos derived from PWM-based models obtained for SEP3-AG and SEP3-AG^{IAP1}. (D) Predictive power of TFBS models. Models are built using 600 sequences best bound by each of the two heterocomplexes and are searched against 1,073 SEP3-AG (orange) and 1,073 SEP3-AG^{IAP1} (blue) specific regions, defined as the top 15% of sequences that are most strongly bound by one complex relative to the other. Matrix-based models (PWM and TFFM) are not able to differentiate SEP3-AG and SEP3-AG^{IAP1} binding whereas k-mer-based analysis is able to better predict binding for the respective datasets. (E) SEP3-AG favors intersite spacings of 47 and 57 bp based on SEP3-AG specific regions. SEP3-AG^{IAP1} favors intersite spacings of 25 and 34 bp based on SEP3-AG^{IAP1} specific regions. (F) Top, published SELEX-seq for SEP3-AP1 and SEP3-AG⁵ comparing the normalized score ratios (SEP3-AG/SEP3-AP1) for SELEX-seq and score ratios (AG/AP1) ChIP-seq at 1,500 SEP3 best bound loci in ChIP-seq show a positive correlation, suggesting that SEP3-AP1 and SEP-AG bind different sequences *in vivo* and that *in vitro* binding is able to differentiate bound sequences that are more SEP3-AP1-like versus SEP3-AG-like. Bottom, SEP3-AG and SEP3-AG^{IAP1} seq-DAP-seq coverage as per SELEX-seq scores. A positive correlation is observed suggesting that, *in vitro*, the swap of AP1 I domain in AG is able to recover some of the binding specificity of SEP3-AP1. (G) Yeast two-hybrid assays using AG, AP1 and AG^{IAP1} as bait against MIKC^C MADS TFs in Arabidopsis. Data shows that AG^{IAP1} loses AG interactors and gains AP1 interactors.

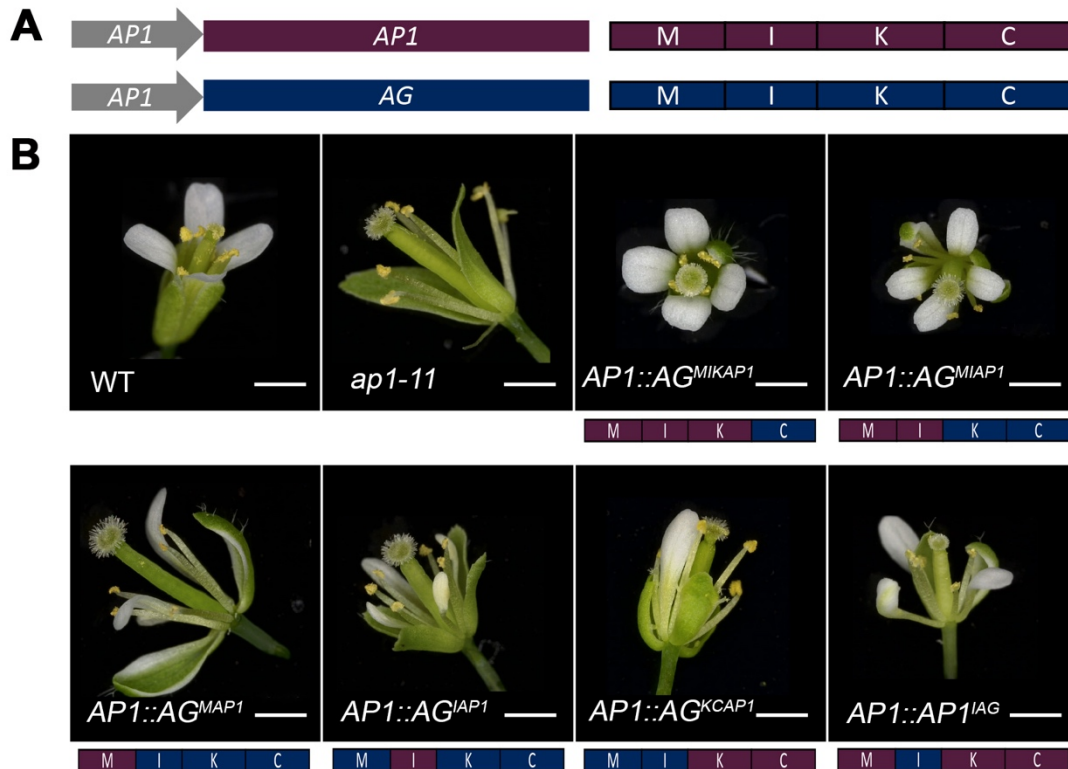
311 **Impact of the I domain on protein interaction specificity**

312 Next, we sought to understand to what extent the I domain could confer protein-
313 protein interaction specificity as it plays an important role in dimerization and dimer
314 stability²⁸. AP1 and AG share SEP3 as a binding partner in the molecular model predicting
315 flower organ specification, but do exhibit differential heterodimerisation capabilities with
316 other MIKC^c MADS TFs^{14,23}. In order to probe the function of the I domain in dimerization
317 specificity, a matrix-based yeast two-hybrid screen for AP1, AG and AG^{IAP1} against all
318 Arabidopsis type II MIKC^c MADS TFs was performed. The targets were cloned into both bait
319 and prey vectors and only interactors for both replica and in all three selection media were
320 scored as positive interactions (**Supplementary Figure 4**). This may underestimate the true
321 number of binding partners, however, it reduces the number of false positives. Using this
322 strict cut-off for protein-protein interaction events, AP1 interacted with seven different
323 partners, of which three were specific for AP1 and four were in common with AG, including
324 the SEP clade members SEP1 and SEP3. AG interacted with ten partners of which six were
325 exclusive with respect to AP1 interacting partners. AG^{IAP1} interacted with ten partners,
326 including two out of the three AP1-specific interactions and lost four AG-specific partners
327 (**Figure 4G**). Interestingly, both SOC1 and AGL24, known AP1 binding partners¹⁴ interacted
328 with the AG^{IAP1} chimera but not with AG. These data indicate that the I domain of AP1
329 contributes to heterodimerization specificity of the chimera.

330

331 **In planta function of the I domain**

332 *Apl* mutants (strong *apl-7* and intermediate *apl-11*) exhibit a non-ambiguous flower
333 phenotype including the homeotic conversion of the first whorl sepals into bract-like organs,
334 as characterized by their leaf-like epidermal morphology and the formation of buds in their
335 axils and the absence of second whorl organs (**Supplementary Figure 5**)^{46,47}. To examine the
336 role of the I domain in *in vivo* MADS function, complementation of the *apl* loss-of-function
337 mutants with different AG/AP1 chimeric constructs was examined. Primary transformants
338 expressing a battery of chimeric domain swap constructs, AG^{MIKAP1}, AG^{MIAP1}, AG^{MAP1}, AG^{IAP1},
339 AG^{KCAP1} and AP1^{IAG}, under the control of the *API* promoter, revealed a spectrum of
340 complementation for the first and second whorls in the intermediate *apl-11* mutant
341 background (**Figure 5**).



342
343
344
345
346
347

Figure 5. Primary transformants in the *ap1* mutant background exhibit a spectrum of complementation. (A) Schematic of the constructs and proteins produced with AP1 protein in purple and AG in dark blue. Domains are labeled MIKC. **(B)** Flower phenotypes of T1 transformants ($n \geq 10$). All transformants were in the *ap1-11* background. Phenotypes for WT and *ap1-11* are shown. The domains corresponding to AP1 and AG are colored as per (A) and shown schematically below each panel.

348

349

350

351

352

353

354

355

356

357

358

359

360

AG^{MAP1} expressing plants were poorly complemented with a reduced number of first and second whorl organs and only partial organ identity recovery with petaloid and sepaloid organs in 43% of the plants. *AG*^{KCAP1} also complemented poorly, with most of the plants showing carpeloid sepals and with only partial recovery of 1 to 3 sepals in 60% of the plants. In contrast, almost complete complementation was present in plants expressing *AG*^{MIAP1}, with 92% of the transformants showing 4 sepals or petaloid sepals in the first whorl and 2 to 4 petals in the second whorl. This was similar to plants expressing *AG*^{MIKAP1}, in which first and second whorl organ identity was restored for 69% of the plants with occasional reduced number of organs in the second whorl and lateral flower formation. *AP1* plants with the I domain of AG (*AP1*^{IAG}), showed a similar phenotype as *AG*^{MAP1}. Strikingly, *AG*^{IAP1} expressing plants exhibited 4 sepaloid organs and 3-4 petals or petaloid organs in over 40% of the plants, suggesting that the I domain acts as the smallest unit conferring the most AP1 function to the *AG*^{IAP1} chimera (**Supplementary Table 2**).

361

362

To confirm the phenotype of the *AG*^{IAP1} expressing plants, three independent homozygous lines were generated and examined for *AP1*, *AG* and *AG*^{IAP1} under the *AP1*

363 promoter in the strong *ap1-7* mutant background (**Figure 6 and Supplementary Figures 6-**
 364 **8**). AG^{IAP1} *ap1-7* lines produced flowers very similar to WT (**Figure 6**).

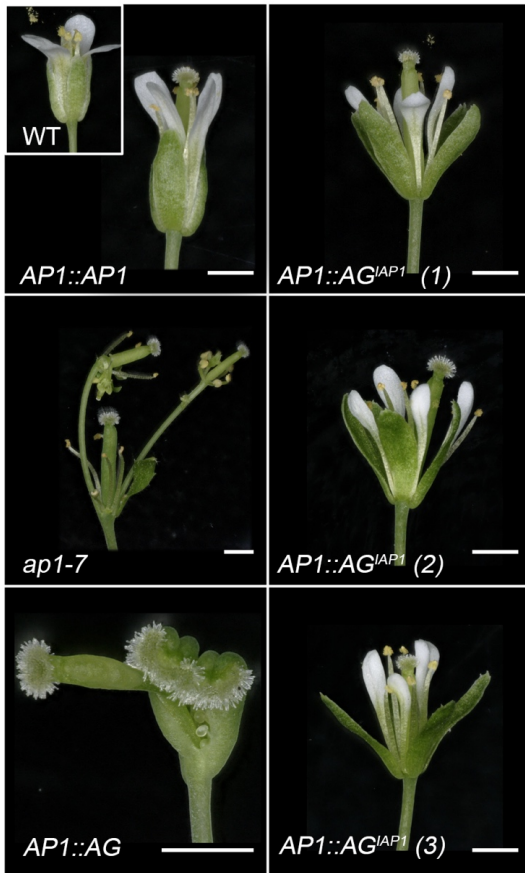
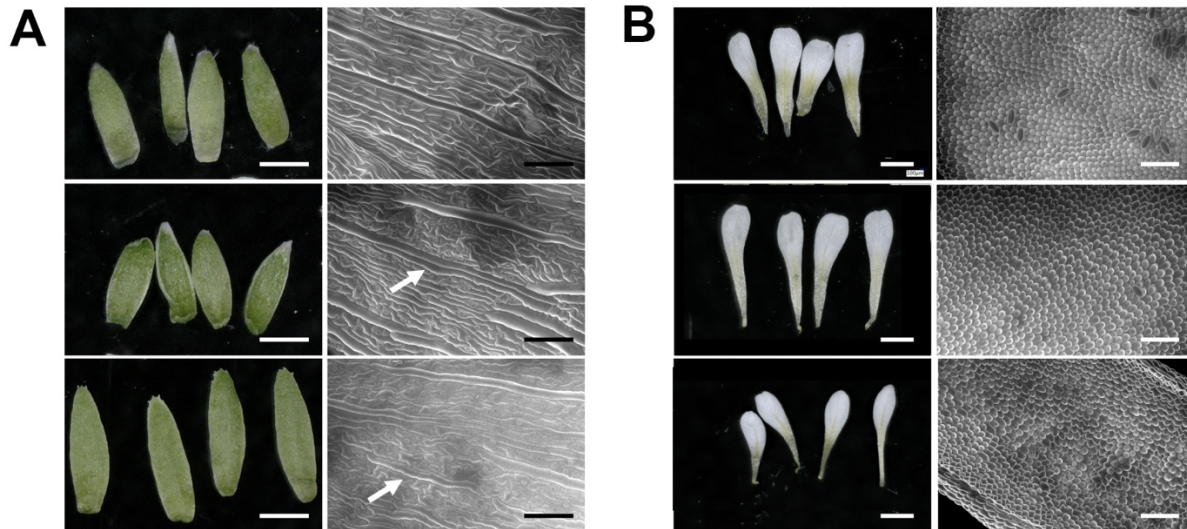


Figure 6. $AP1:AG^{IAP1}$ expression largely complements the *ap1-7* flower phenotype. *ap1-7* lines expressing either *AP1* ($AP1::AP1$), *AG* ($AP1::AG$) or AG^{IAP1} ($AP1::AG^{IAP1}$) under the control of the *AP1* promoter were grown at 22 °C in long days. A typical WT flower is shown as an insert in the upper left panel. Representative flowers for 3 independent $AP1::AP^{IAP1}$ lines are presented and one representative flower from $AP1::AG$ and $AP1::AP1$ expressing lines. While the first whorl in *ap1-7* is replaced by bract or stipule with axillary buds and petals are missing in the second whorl, $AP1::AG^{IAP1}$ expression restores WT first and second whorl organs, while *AG* expression triggers carpel development in the first whorl and absence of petals in the second whorl. Scales bars = 1 mm.

365
 366 In these plants, whorl 1 of each flower was made of four sepal-like organs and axillary
 367 buds were never observed as opposed to the *ap1-7* mutant (**Figure 6 and 7**). In addition,
 368 between 66% to 82% of the flowers in three independent lines homozygous for the transgene
 369 showed 4 petal-like organs (**Figure 6 and 7**). Scanning electron microscopy (SEM)
 370 observations of epidermal cells from whorls 1 and 2 of AG^{IAP1} expressing lines showed
 371 elongated cells characteristic of sepals and conical cells characteristic of petals, respectively
 372 (**Figure 7 and Supplementary Figure 7**). Detailed inspection of sepal and petal surfaces by
 373 SEM from the AG^{IAP1} expressing plants revealed the presence of a few clusters of leaf-like
 374 and stamen identity cells in whorls 1 and 2, respectively (**Figure 7 and Supplementary**
 375 **Figure 8**). In these 3 lines, 10 to 25% of the flowers showed petals with only petal identity
 376 cells while 75 to 90% of the flowers show at least one petal with a small cluster of stamen
 377 identity cells (**Supplementary Figure 8**). This indicates incomplete complementation of *AP1*
 378 function by the chimera. However, $AP1:AG$ was unable to even partially complement *AP1*
 379 function in the first and second whorl. Inspection of the cell surface in *ap1-7* $AP1:AG$ plants
 380 of the first whorl showed characteristic carpel cells (replum, style and papilla) and an absence

381 of organs in the second whorl (**Supplementary Figure 6**). AG^{IAP1} therefore possesses the
 382 ability to trigger *API* specific developmental programs and has lost much of its ability to
 383 trigger *AG*-specific organ development, indicating that the I domain of AP1 plays a major role
 384 in conferring AP1 functional identity to AG^{IAP1} *in vivo*.



385
 386 **Figure 7. First and second whorls cell identity are complemented in *ap1-7* plants expressing AG^{IAP1} .** First (A) and
 387 second (B) whorl organs were removed from WT, and flowers from *API* or AG^{IAP1} expressing *ap1-7* plants. First whorl
 388 organs in AG^{IAP1} expressing plants are slightly longer compared to WT and *API* expressing plants (A, left panel). Second
 389 whorl organs in AG^{IAP1} expressing plants are slightly smaller compared to WT and *API* expressing plants (B, left panel).
 390 Epidermal cell identity, observed by SEM, show characteristic WT elongated sepal cells in *API* and AG^{IAP1} expressing plants
 391 (A, right panel) and characteristic WT conical cells in petals from *API* and AG^{IAP1} expressing plants (B, right panel). A small
 392 number of epidermal cells typical of leaves are also seen in AG^{IAP1} expressing plants and to a lesser extent in *API* expressing
 393 plants (arrow). Scale bars indicate 100 μ M for SEM images and 1 mm for organ photographs.

394 Discussion

395 Transcription factor function depends on its selective binding of specific sequences in
 396 the genome. The MADS TF family has dramatically expanded in the green lineage over the
 397 course of evolution and fulfills many roles throughout the lifecycle of the plant. MADS
 398 constitute one of the largest plant TF families and are almost evenly divided into two types, I
 399 and II, represented structurally by SRF and MEF2. The MADS-box DBD, encoded by a
 400 single exon, is either SRF-like or MEF2-like and exhibits little sequence variation even
 401 amongst different eukaryotic kingdoms of life. How the MADS TF family is able to regulate
 402 diverse developmental processes and different target genes with such a highly conserved
 403 DBD has been a fundamental question leading to the speculation that regions distal to the
 404 DBD may play a role in DNA-binding specificity either via the formation of higher order
 405 complexes, the recruitment of ternary factors or via allosteric alterations in DNA-binding
 406 specificity of the MADS-box domain.

407 Domain swap experiments performed over 25 years ago suggested that the I domain

408 played a key role in DNA-binding specificity and dimerization in floral organ identity MADS
409 TFs, although the mechanism of this was unclear^{29,43,48}. Based on the *in vitro* and *in vivo* data
410 presented here, the I region or I domain should be considered as a fundamental component of
411 the DNA-binding module as it is essential for DNA-binding for both type I and II MADS
412 TFs. Examination of the structure of the MI domains of SEP3 in comparison with MEF2 and
413 SRF coupled with secondary structure predictions, reveals that the I region is always alpha
414 helical and interacts extensively with the beta sheet of the M domain, albeit with different
415 orientations. This suggests that allosteric effects of the I region in type I and II MADS TFs,
416 due to variability in amino acid composition, length and secondary structure orientation, will
417 influence the MADS-domain conformation and tune DNA-binding and specificity. In
418 addition, the I region alters dimer partner specificity, altering the repertoire of heteromeric
419 MADS complexes able to be formed and resulting in additional functional diversity *in vivo*.

420 With the introduction of the floral quartet model, the role of the I domain in
421 determining MADS TF function specificity was supplanted by the importance of specific
422 tetramer components triggering DNA-looping as being required for gene regulation²⁴.
423 Tetramerisation allows cooperative two-site binding and looping of DNA, thus selecting for
424 DNA-binding sites that exhibit preferred spacing^{31,34,49,50}. Examination of a tetramerisation
425 mutant of SEP3 revealed that fourth whorl carpel development and meristem determinacy
426 require efficient tetramerisation of SEP3³³. Recent studies comparing the genome-wide
427 binding patterns of tetrameric versus dimeric SEP3-AG complexes have further shown that
428 tetramerisation both increases binding affinity and plays a role in determining DNA-binding
429 specificity via preferential binding of specific intersite distances³². Comparisons of genome-
430 wide binding of SEP3-AG and SEP3-AG^{IAPI}, presented here, reveals that the I domain alters
431 preferred intersite spacing between CARG-type binding sites. These data suggest a role of the
432 I domain as a modulator of tetramerisation and highlight an additional mechanism mediated
433 by the I domain for changing DNA binding patterns of MADS TF complexes.

434 The recruitment of ternary factors, non-MADS family protein partners, has been
435 postulated to be a major determinant of DNA-binding specificity⁵¹. Based on yeast 2-hybrid
436 screening, mass spectrometry and pulldown assays, additional TF partners from the NF-Y and
437 homeodomain families as well as the orphan TF, LEAFY, have been identified for a few type
438 II MADS TFs including OsMADS18 from rice and SHATTERPROOF, SEEDSTICK, AG
439 and SEP3 from Arabidopsis^{25,48,52,53}. While ternary complex formation likely plays a role in
440 differential gene regulation, the formation of such complexes has only been shown for a
441 relatively small number of MADS TFs and how much it accounts for the diversity of function

442 in the MADS TF family requires further studies. As shown here, swapping the I domain of the
443 well-studied floral organ identity MADS TF, AP1 (first and second whorl organs) into the
444 third and fourth whorl specific TF, AG, results in strong complementation of the *apl* loss of
445 function phenotype by the chimeric construct. The experiments keep the K and C-terminal
446 domains of AG intact and these domains have been postulated to be important for neo-
447 functionalization⁵⁴ and/or the recruitment of ternary factors⁵⁵. We cannot completely exclude
448 that ternary factors recruited via the I domain could be responsible for the *API*-like activity of
449 *AG^{IAP1}* in planta. For example, OsMADS18 uses the MI domains to recruit OsNF-YB1 based
450 on yeast 2-hybrid assays⁴⁸. However, it is more likely that the combination of tuning DNA-
451 binding specificity and heterodimer partner selection by the I domain accounts for the
452 majority of AP1 activity of the *AG^{IAP1}* chimera.

453 Based on the *in vitro* and *in vivo* experiments presented here, the I region is absolutely
454 required for DNA-binding with the minimal DNA binding domain consisting of the M plus
455 the I region, as opposed to the M domain alone. As shown here, the I domains of AP1 and AG
456 also play an important role in DNA-binding and dimerization specificity. The I domain is able
457 to tune the function of plant MADS TFs and, in the case of AP1, acts as a major determinant
458 of functional identity in concert with the M domain. Further experiments will be required to
459 determine how generalizable these results are to the wider MADS TF family (type I and II)
460 and whether the I region broadly acts as a primary factor in MADS TF functional identity *in*
461 *planta*.

462 **Methods**

463 **SEP3 MI domain protein expression and purification**

464 SEP3 MI (aa 1-90) was cloned into the pETM41 vector using the NcoI-NotI restriction sites
465 to obtain His6-MBP translational protein fusion. Recombinant SEP3 MI protein was
466 expressed in *E. coli* BL 21 Codon Plus cells. Cell were grown at 37 °C to an OD₆₀₀ of 0.8-1
468 after which time the temperature was reduced to 15 °C and protein expression induced by
469 addition of 1 mM of IPTG for 12 h. Cells were harvested by centrifugation and the cell pellet
470 resuspended in 25 mM KH₂PO₄ pH 7 buffer containing 10 % glycerol, 500 mM NaCl, 2 mM
471 Tris(2-carboxyethyl)phosphine (TCEP) and cOmplete protease inhibitors (Roche). Cells were
472 lysed by sonication and cell debris pelleted at 25,000 rpm for 40 min. The soluble fraction
473 was applied to a 1 ml Ni-NTA column and the protein eluted with resuspension buffer + 200
474 mM imidazole. The protein was dialysed against 25 mM Tris, pH 8.0, 300 mM NaCl and 1
475 mM TCEP. The protein was then applied to a heparin column to remove any bound DNA
476 using a salt gradient from 300 mM to 2 M NaCl. The protein was dialysed overnight in the
477 presence of TEV protease (10:1) to cleave the His-MBP tag at 4 °C. The protein was then
478 passed over a Ni-NTA column to deplete the His-MBP and any uncleaved protein. A second
479 heparin column was run to remove any His-MBP and to obtain pure SEP3 MI. The protein
480 was concentrated to ~6 mg/ml and used for crystallization trials.

481

482 **Protein crystallization, data collection and refinement**

483 SEP3 MI at a concentration of 6 mg/ml was mixed at a 1:1 ratio with potassium sodium
484 tartrate tetrahydrate (0.2 M), bis-tris propane (0.1 M, pH 7.5) and 20 % PEG 3350. The
485 protein crystallized over 20 d at 4 °C forming a diamond shaped single crystal. 15 % glycerol
486 was used as a cryoprotectant and the crystal flash frozen in liquid N₂. Diffraction data were
487 collected at 100 K at the European Synchrotron Radiation Facility (ESRF), Grenoble France
488 on ID29 at a wavelength of 1.0 Å. Indexing was performed using MXCube⁵⁶ and the default
489 optimized oscillation range and collection parameters used for data collection. The data set
490 was integrated and scaled using the programs *XDS* and *XSCALE*⁵⁷. Data collection and
491 refinement statistics are given in Table 1. The structure is deposited under PDB code 7NB0.

492

493 **In vitro pull-down assays**

494 The following constructs from type I and type II MADS TFs are cloned into pTnT vector for
495 in vitro pulldown assays. Type I MADS TFs include AGL61^{MI}(63-122)-5MyC, AGL61^{MI}(63-
496 155)-5MyC, PHE^{MI}(1-60)-3FLAG, PHE^{MI}(1-95)-3FLAG, AGL80^{MI}(1-61)-3FLAG and
497 AGL80^{MI}(1-88)-3FLAG, and type II MADS TFs include SEP3^{MI}(1-57)-3FLAG, SEP3^{MI}(1-
498 90)-3FLAG, AG^{MI}(1-73)-5MyC, AG^{MI}(1-107)-5MyC, AG(ΔN)^{MI}(17-73)-5MyC,
499 AG(ΔN)^{MI}(17-107)-5MyC, AP1^{MI}(1-57)-5MyC and AP1^{MI}(1-92)-5MyC. Proteins were
500 produced using in vitro transcription and translation system using wheat germ extract
501 following manufactures' instructions (SP6 High Yield Expression System from Promega).
502 Briefly, purified plasmids were used as input in a 2 hr 25 °C incubation reaction. For single
503 input reactions, 1 μg of plasmid was used in a 25 μl reaction volume. For double input
504 reactions, 1 μg plasmid of each construct was used in a 25 μl reaction volume. 10 % of each
505 input reaction (i.e. 2.5 μl) was used as input for western blots. The rest of the reaction was
506 used for pull-down experiments. Briefly, each reaction was completed to 100 μl using PBS
507 buffer (150 mM sodium phosphate, pH 7.2, and 150 mM NaCl), and added with 10 μl of the
508 appropriate magnetic beads (anti-MyC beads, Thermo Fisher or anti-FLAG beads, Merck
509 Millipore) and incubated for 1 hr at 4 °C. The beads plus protein solution suspension was then
510 placed on magnets, and the supernatant was discarded. The beads were washed with PBS
511 buffer four times, and SDS-PAGE loading dye was added to the beads and boiled for 5 min.
512 at 95 °C. Western blots were used to assess the pulldown results using anti-MyC (Thermo
513 Fisher) and anti-FLAG antibodies (Merck Millipore).

514

515 **EMSA experiments**

516 Proteins for EMSAs experiments were produced as described above. EMSAs were performed
517 as described with 10 nM DNA labeled with Cy5 (Eurofins) using a 103-bp DNA fragment
518 containing 2 CA₂G boxes belonging to the *SEP3* promoter³³. For each EMSA, a negative
519 control was run, labeled 'DNA alone' in which the in vitro translation assay was done with
520 pTNT vector without any insert and incubated with the DNA probe.

521

522 **Yeast two-hybrid screening**

523 AP1, AG and the chimeric construct, AG^{IAP1} (residues 74-107 of AG replaced by residues 58-
524 92 of AP1) were cloned into pENTR/D-TOPO® (Kan) gateway entry vector. Subsequently,
525 Gateway LR reactions were performed using pDEST32 (pBDGAL4) and pDEST22
526 (pADGAL4) destination vectors. The resulting pDEST32-AG, pDEST32-AP1 or pDEST32-
527 AG^{IAP1} expression construct was transformed into yeast strain PJ69-4α, and pDEST22-AG,
528 pDEST22-AP1 or pDEST22-AG^{IAP1} into PJ69-4A, followed by an autoactivation screen for
529 the bait vector as described⁵⁸. Upon confirmation that the AG^{IAP1} bait did not possess any
530 autoactivation capacity, a matrix-based Y2H screening was performed following the protocol
531 described in⁵⁸. Bait and prey clones of all native Arabidopsis type II MIK^c MADS TFs were

532 generated previously¹⁴ and were screened against AP1, AG and AG^{IAP1}. Growth of yeast and
533 hence, protein-protein interaction events, were scored after seven days of incubation at 20 °C
534 on selective medium. Three different selective media were used: SD lacking Leucine,
535 Tryptophan, and Histidine (-LWH) and supplemented with 1 mM 3-Amino-1,2,4-triazole (3-
536 AT); SD -LWH + 5 mM 3-AT and SD lacking L,W and Adenine (-LWA). Mating was
537 performed twice in independent experiments and only combinations of MADS TFs giving
538 growth on all three selection media and in both replica were scored as interaction events.
539

540 **Seq-DAP-seq**

541 Seq-DAP-seq for SEP3-AG^{IAP1} complex was performed as described previously³². Briefly, 2
542 µg of each purified plasmid (pTnT-SEP3-3FLAG and pTnT- AG^{IAP1}-5MyC) were used as
543 input in a 50 µl TnT reaction incubated at 25 °C for 2 hr (Promega). The reaction solution was
544 then combined with 50 µl IP buffer (PBS supplemented with 0.005 % NP40 and proteinase
545 inhibitors (Roche)) and mixed with 20 µl anti-FLAG magnetic beads (Merck Millipore).
546 Following 1 hr. incubation at room temperature, the anti-FLAG magnetic beads were
547 immobilized, and washed three times with 100 µl IP buffer. Protein complexes were eluted
548 with 100 µl IP buffer supplemented with 200 µg/ml 3xFLAG peptide (Merck Millipore). The
549 eluted protein was then immobilized on anti-c-Myc magnetic beads (Thermo Fisher) and
550 washed three times with 100 µl IP buffer to isolate homogeneous SEP3-AG^{IAP1} complex. The
551 purified protein complex, while still bound on anti-c-Myc magnetic beads, was incubated with
552 50 ng DAP-seq input library pre-ligated with Illumina adaptor sequences. The reaction was
553 incubated for 90 mins, and then washed 6 times using 100 µl IP buffer. The bound DNA was
554 heated to 98 °C for 10 min and eluted in 30 µl EB buffer (10 mM Tris-Cl, pH 8.5). The eluted
555 DNA fragments were PCR amplified using Illumina TruSeq primers for 20 cycles, and
556 purified by AMPure XP beads (Beckman). The libraries were quantified by qPCR, pooled and
557 sequenced on Illumina HiSeq (Genewiz) with specification of paired-end sequencing of 150
558 cycles. Each library obtained 10 to 20 million reads. The seq-DAP-seq was performed in
559 triplicate.
560

561 **Seq-DAP-seq data analysis**

562 *Reads processing and peak calling*

563 SEP3-AG and SEP3-AG^{IAP1} reads processing and peak calling was performed as previously
564 described³². Briefly, reads were checked using FastQC
565 (<http://www.bioinformatics.babraham.ac.uk/projects/fastqc/>) and adapter sequences removed
566 with NGmerge⁵⁹ and mapped with bowtie2⁶⁰ onto the TAIR10 version of the *A. thaliana*
567 genome (www.arabidopsis.org), devoid of the mitochondrial and the chloroplast genomes.
568 The duplicated reads were removed using the samtools rmdup program⁶¹. The resulting
569 alignment files for each sample were input to MACS2⁶² to call peaks using the input DNA as
570 control. Consensus peaks between replicates were defined using MSPC⁶³ (P-value cutoff =
571 10⁻⁴) for each experiment. Each consensus peak was scanned for possible subpeaks, split into
572 several peaks if needed, and the peak widths were then re-sized to ± 200 bp at both side of the
573 peak maximal height. For all the resulting peaks, coverage was computed as the mean of the
574 normalized read coverage for each replicate. This normalized coverage defines the binding
575 intensity of a heterocomplex at a bound region.
576

577 *Comparison between SEP3-AG and SEP3-AG^{IAP1}*

578 SEP3-AG or SEP3-AG^{IAP1} were merged according to the following procedure: peaks were
579 considered common if at least 80 % of two peaks overlapped with < 50 % of either peak non-
580 overlapping. Peaks that did not overlap by > 50 % of their length were considered new peaks.
581 These values were chosen empirically based on visual inspection of the peaks in the

582 Integrated Genome Browser⁶⁴. The averaged normalized coverage from each experiment,
583 divided by the peak size, was computed for each peak. Figure 4 was computed using R
584 (<https://www.Rproject.org>) and the ggplot library⁶⁵. The coverage fold reduction (CFR) was
585 computed as the ratio between the mean normalized coverages in SEP3-AG^{IAP1} and SEP3-
586 AG seq-DAP-seq. The top 15 % sequences with extremes CFR were considered SEP3-
587 AG^{IAP1} and SEP3-AG specific and used to search for differential DNA patterns that
588 potentially direct transcription factor differential binding using sequence modelling (see next
589 paragraph). Detection of preferred spacings between canonical CArG boxes was performed as
590 in ³².

591

592 *Position weight matrices (PWM), transcription factor flexible model (TFFM) and k-mer set*
593 *memory (KSM).*

594 For each experiment, PWM, TFFM and KSM models were reconstructed out of the 600 best
595 peaks (judged according to their averaged coverage). PWM were generated by the meme-
596 suite, using meme-chip⁶⁶ with options -meme-minw 16, -mememaxw 16, -meme-nmotifs 1 –
597 meme-pal. TFFM were generated using the TFFM-framework package and the PWM
598 obtained in the meme-chip output ⁶⁷. KSM is a recently developed TF binding motif
599 representation that consist of a set of aligned k-mers that are overrepresented at TF binding
600 sites. KSM were generated using the KMAC tool ⁴⁵ with options set to search k-mers, with
601 size ranging from 4 to 20bp in a 300bp sliding windows, that are enriched compare to TF
602 unbound sequences. TF binding sites were predicted by searching the PWM, TFFM and KSM
603 models against TF bound sequences and unbound sequences. PWM and TFFM scan was
604 performed using in house scripts. KSM were searched using the KSM tool ⁴⁵. The best
605 TFFM/PWM scores and the sum of KSM scores (because distinct KSM can hit to a same
606 subject sequence) obtained for each bound regions and for unbound regions are retained to
607 assess the prediction power of each model in an AUROC (Area Under the Receiver Operating
608 Characteristic Curve). In this assessment, the unbound set of regions are chosen with similar
609 GC content, size, and origin (promoter, intron, exon and intergenic) than the set of bound
610 regions ⁶⁸. The set of unbound sequences fed to KMAC to detect enriched k-mer is different
611 than the one used to evaluate the KSM model prediction.

612

613 **Plant material and growth conditions**

614 All experiments were performed using *A. thaliana* Col-0 accession. *Ap1-7* allele was obtained
615 from cal/cal all-7 plants kindly provided by Justin Goodrich and the *ap1-11* (N6231) mutant
616 was ordered from the Nottingham Arabidopsis Stock Centre. Seedlings were grown in
617 controlled growth chambers in long day conditions (16 h light / 8 h dark) at 22 °C for plant
618 transformation and phenotype analysis. WT, *ap1* mutant and complemented lines were always
619 grown in parallel.

620

621 **Plasmid constructs for plant transformation**

622

623 Constructs used for the primary transformant phenotypic analysis were cloned into a modified
624 version of pMDC32 binary vector⁶⁹, where the 2x35S promoter was replaced with the *API*
625 promoter. *AG^{MAP1}*, *AG^{MIAP1}*, *AG^{MIKAP1}*, *AG^{KCAP1}*, *AG^{CAP1}*, *API^{IAG}* and *AG^{IAP}* coding sequences
626 were amplified from pTNT-*AG^{MAP1}*, pTNT-*AG^{MIAP1}*, pTNT-*AG^{MIKAP1}*, pTNT-*AG^{KCAP1}*, pTNT-
627 *AG^{CAP1}*, pTNT-*API^{IAG}* and pTNT-*AG^{IAP}* vectors and subsequently inserted by XbaI restriction
628 enzyme downstream of the *API* promoter. pTNT-CDS vectors were generated through
629 Gibson assembly (NEB).

630

631 *API::API*, *API::AG* and *API::AG^{LAPI}* vectors were generated using Gibson assembly in the
632 vector backbone pFP100⁷⁰. *API* promoter and *OCT* terminator were PCR amplified from
633 pML-BART-AP1pro:AP1-AR plasmid⁷¹. *API*, *AG* and *AG^{LAPI}* coding sequences were
634 amplified from pTNT-*API*, pTNT-*AG*, pTNT- *AG^{LAPI}* vectors.
635

636 **Plant transformation and floral phenotype analysis**

637

638 All the plant transformations were performed using *apl* mutant plants following the floral dip
639 method⁷². For primary resistant analysis in *apl-11* intermediate allele, T1 seeds were sown on
640 the 0.5X MS medium supplemented with 20 µg/ml hygromycin. Resistant plants were
641 transferred to soil. Flowers arising from the primary shoot were analyzed by light microscopy.
642 For the detailed analysis of the *API::API*, *API::AG* and *API::AG^{LAPI}*, the strong allele *apl-7*
643 was used as transformation background and T1 seeds were selected based on the seed specific
644 GFP selection marker⁷⁰. Flower phenotypic analyses were performed by light microscopy on
645 flower number ~10 to 19 based on their order of emergence on more than 20 T1 plants for
646 each construct, growing in parallel to *apl-7* plants. Three independent lines with one insertion
647 expressing *AG*, *API* and *AG^{LAPI}* were selected for further phenotype analyses.
648

649 **Environmental scanning electron microscopy**

650

651 SEM experiments were performed at the Electron Microscopy facility of the ICMG Nanobio-
652 Chemistry Platform (Grenoble, France) as described³³.
653
654

655

656 **Table 1.**

657

658 **Data collection and refinement statistics**

659

	SEP3 ^{MI}
Data collection	
Space group	C222 ₁
Cell dimensions	
<i>a</i> , <i>b</i> , <i>c</i> (Å)	67.4, 67.4, 122.6
α , β , γ (°)	90, 90, 90
Resolution (Å)	48.-2.10 (2.16-2.10) *
<i>R</i> _{sym} or <i>R</i> _{merge}	8.4 (130)
<i>CC</i> _{1/2}	99.8 (56.4)
Completeness (%)	99.0 (95.6)
Redundancy	6.0 (4.1)
Refinement	
Resolution (Å)	47.7-2.10
No. reflections	16519
<i>R</i> _{work} / <i>R</i> _{free} (%)	20.4/23.6 (32.8/34.2)*
No. atoms	1880
Protein	1814
Ligand/ion	0
Water	66
<i>B</i> -factors	
Protein	55.5
Water	53.6
R.m.s. deviations	
Bond lengths (Å)	0.008
Bond angles (°)	1.24

660

661 • refers to highest resolution shell

662

663 **Funding:** This project received support from the ANR (ANR-16-CE92-0023) and the GRAL
664 LabEX (ANR-10-LABX-49-01) with the frame of the CBH-EUR-GS (ANR-17-EURE-0003).
665 This work benefited from access to the MX-Grenoble, an Instruct-ERIC centre within the
666 Grenoble Partnership for Structural Biology (PSB). Financial support was provided
667 by Instruct-ERIC (PID 13317), FRISBI (ANR-10-INBS-05-02) and GRAL, a programme
668 from the Chemistry Biology Health (CBH) Graduate School of University Grenoble Alpes
669 (ANR-17-EURE-0003).

670

671 **Author contributions:** KK, FP, VH, CS and CZ conceived the study, CS, VH, RI, FP and CZ
672 designed experiments, XL, RVL, CSS, AJ and VH performed experiments, RBM, JL and JM
673 analyzed data, CZ wrote the manuscript with the help of all authors.

674

675

676 **References**

- 677 1 Passmore, S., Maine, G. T., Elble, R., Christ, C. & Tye, B. K. Saccharomyces
678 cerevisiae protein involved in plasmid maintenance is necessary for mating of MAT
679 alpha cells. *J Mol Biol* **204**, 593-606, doi:10.1016/0022-2836(88)90358-0 (1988).
- 680 2 Yanofsky, M. F. *et al.* The protein encoded by the Arabidopsis homeotic gene
681 agamous resembles transcription factors. *Nature* **346**, 35-39, doi:10.1038/346035a0
682 (1990).

- 683 3 Sommer, H. *et al.* Deficiens, a homeotic gene involved in the control of flower
684 morphogenesis in *Antirrhinum majus*: the protein shows homology to transcription
685 factors. *EMBO J* **9**, 605-613 (1990).
- 686 4 Norman, C., Runswick, M., Pollock, R. & Treisman, R. Isolation and properties of
687 cDNA clones encoding SRF, a transcription factor that binds to the c-fos serum
688 response element. *Cell* **55**, 989-1003, doi:10.1016/0092-8674(88)90244-9 (1988).
- 689 5 Smaczniak, C., Angenent, G. C. & Kaufmann, K. SELEX-Seq: A Method to
690 Determine DNA Binding Specificities of Plant Transcription Factors. *Methods Mol*
691 *Biol* **1629**, 67-82, doi:10.1007/978-1-4939-7125-1_6 (2017).
- 692 6 Martinez-Castilla, L. P. & Alvarez-Buylla, E. R. Adaptive evolution in the
693 Arabidopsis MADS-box gene family inferred from its complete resolved phylogeny.
694 *Proc Natl Acad Sci U S A* **100**, 13407-13412, doi:10.1073/pnas.1835864100 (2003).
- 695 7 Alvarez-Buylla, E. R. *et al.* An ancestral MADS-box gene duplication occurred before
696 the divergence of plants and animals. *Proc Natl Acad Sci U S A* **97**, 5328-5333,
697 doi:97/10/5328 [pii] (2000).
- 698 8 Pollock, R. & Treisman, R. Human SRF-related proteins: DNA-binding properties and
699 potential regulatory targets. *Genes Dev* **5**, 2327-2341 (1991).
- 700 9 Huang, H., Mizukami, Y., Hu, Y. & Ma, H. Isolation and characterization of the
701 binding sequences for the product of the Arabidopsis floral homeotic gene
702 AGAMOUS. *Nucleic Acids Res* **21**, 4769-4776 (1993).
- 703 10 Wynne, J. & Treisman, R. SRF and MCM1 have related but distinct DNA binding
704 specificities. *Nucleic Acids Res* **20**, 3297-3303, doi:10.1093/nar/20.13.3297 (1992).
- 705 11 Shiraishi, H., Okada, K. & Shimura, Y. Nucleotide sequences recognized by the
706 AGAMOUS MADS domain of Arabidopsis thaliana in vitro. *Plant J* **4**, 385-398
707 (1993).
- 708 12 Pellegrini, L., Tan, S. & Richmond, T. J. Structure of serum response factor core
709 bound to DNA. *Nature* **376**, 490-498, doi:10.1038/376490a0 (1995).
- 710 13 De Bodt, S. *et al.* Genomewide structural annotation and evolutionary analysis of the
711 type I MADS-box genes in plants. *J Mol Evol* **56**, 573-586, doi:10.1007/s00239-002-
712 2426-x (2003).
- 713 14 de Folter, S. *et al.* Comprehensive interaction map of the Arabidopsis MADS Box
714 transcription factors. *Plant Cell* **17**, 1424-1433, doi:tpc.105.031831 (2005).
- 715 15 Masiero, S., Colombo, L., Grini, P. E., Schnittger, A. & Kater, M. M. The emerging
716 importance of type I MADS box transcription factors for plant reproduction. *Plant*
717 *Cell* **23**, 865-872, doi:10.1105/tpc.110.081737 (2011).
- 718 16 Bemer, M., Heijmans, K., Airoidi, C., Davies, B. & Angenent, G. C. An atlas of type I
719 MADS box gene expression during female gametophyte and seed development in
720 Arabidopsis. *Plant Physiol* **154**, 287-300, doi:pp.110.160770 (2010).
- 721 17 Saedler, H., Becker, A., Winter, K. U., Kirchner, C. & Theissen, G. MADS-box genes
722 are involved in floral development and evolution. *Acta Biochim Pol* **48**, 351-358
723 (2001).
- 724 18 Becker, A. & Theissen, G. The major clades of MADS-box genes and their role in the
725 development and evolution of flowering plants. *Mol Phylogenet Evol* **29**, 464-489,
726 doi:S1055790303002070 [pii] (2003).
- 727 19 Kaufmann, K., Melzer, R. & Theissen, G. MIKC-type MADS-domain proteins:
728 structural modularity, protein interactions and network evolution in land plants. *Gene*
729 **347**, 183-198, doi:S0378-1119(04)00762-0 (2005).
- 730 20 Kwantes, M., Liebsch, D. & Verelst, W. How MIKC* MADS-box genes originated
731 and evidence for their conserved function throughout the evolution of vascular plant
732 gametophytes. *Mol Biol Evol* **29**, 293-302, doi:10.1093/molbev/msr200 (2012).

- 733 21 Adamczyk, B. J. & Fernandez, D. E. MIKC* MADS domain heterodimers are
734 required for pollen maturation and tube growth in Arabidopsis. *Plant Physiol* **149**,
735 1713-1723, doi:10.1104/pp.109.135806 (2009).
- 736 22 Verelst, W., Saedler, H., Munster, T. MIKC* MADS-Protein complexes Bind Motifs
737 Enriched in the Proximal Region of Pollen-Specific Arabidopsis Promoters. *Plant*
738 *Physiol* **143**, 447-460, doi:<https://doi.org/10.1104/pp.106.089805> (2007).
- 739 23 Immink, R. G. *et al.* SEPALLATA3: the 'glue' for MADS box transcription factor
740 complex formation. *Genome Biol* **10**, R24, doi:gb-2009-10-2-r24 (2009).
- 741 24 Theissen, G. & Saedler, H. Plant biology. Floral quartets. *Nature* **409**, 469-471,
742 doi:10.1038/35054172 (2001).
- 743 25 Smaczniak, C. *et al.* Characterization of MADS-domain transcription factor
744 complexes in Arabidopsis flower development. *Proc Natl Acad Sci U S A* **109**, 1560-
745 1565, doi:10.1073/pnas.1112871109 (2012).
- 746 26 Gramzow, L. & Theissen, G. A hitchhiker's guide to the MADS world of plants.
747 *Genome Biol* **11**, 214, doi:gb-2010-11-6-214 (2010).
- 748 27 Smaczniak, C., Immink, R. G., Angenent, G. C. & Kaufmann, K. Developmental and
749 evolutionary diversity of plant MADS-domain factors: insights from recent studies.
750 *Development* **139**, 3081-3098, doi:10.1242/dev.074674 (2012).
- 751 28 Riechmann, J. L., Krizek, B. A. & Meyerowitz, E. M. Dimerization specificity of
752 Arabidopsis MADS domain homeotic proteins APETALA1, APETALA3,
753 PISTILLATA, and AGAMOUS. *Proc Natl Acad Sci U S A* **93**, 4793-4798,
754 doi:10.1073/pnas.93.10.4793 (1996).
- 755 29 Krizek, B. A. & Meyerowitz, E. M. Mapping the protein regions responsible for the
756 functional specificities of the Arabidopsis MADS domain organ-identity proteins.
757 *Proc Natl Acad Sci U S A* **93**, 4063-4070, doi:10.1073/pnas.93.9.4063 (1996).
- 758 30 Riechmann, J. L. & Meyerowitz, E. M. Determination of floral organ identity by
759 Arabidopsis MADS domain homeotic proteins AP1, AP3, PI, and AG is independent
760 of their DNA-binding specificity. *Mol Biol Cell* **8**, 1243-1259,
761 doi:10.1091/mbc.8.7.1243 (1997).
- 762 31 Jetha, K., Theissen, G. & Melzer, R. Arabidopsis SEPALLATA proteins differ in
763 cooperative DNA-binding during the formation of floral quartet-like complexes.
764 *Nucleic Acids Res* **42**, 10927-10942, doi:10.1093/nar/gku755 (2014).
- 765 32 Lai, X., Stigliani, A., Lucas, J., Hugouvieux, V., Parcy, F., Zubieta, C. Genome-wide
766 binidng of SEPALLATA3 and AGAMOUS complexes dertermined by sequential
767 DNA-affinity purification sequencing. *Nucleic Acids Res* **48**, 9637-9648,
768 doi:10.1093/nar/gkaa729 (2020).
- 769 33 Hugouvieux, V. *et al.* Tetramerization of MADS family transcription factors
770 SEPALLATA3 and AGAMOUS is required for floral meristem determinacy in
771 Arabidopsis. *Nucleic Acids Res* **46**, 4966-4977, doi:10.1093/nar/gky205 (2018).
- 772 34 Puranik, S. *et al.* Structural basis for the oligomerization of the MADS domain
773 transcription factor SEPALLATA3 in Arabidopsis. *Plant Cell* **26**, 3603-3615,
774 doi:10.1105/tpc.114.127910 (2014).
- 775 35 Krissinel, E. & Henrick, K. Inference of macromolecular assemblies from crystalline
776 state. *J Mol Biol* **372**, 774-797, doi:10.1016/j.jmb.2007.05.022 (2007).
- 777 36 Crooks, G. E., Hon, G., Chandonia, J-M., Brenner, S.E. WebLogo:a sequence logo
778 generator. *Genome Res* **14**, doi:10.1101/gr.849004 (2004).
- 779 37 Bemer, M., Wolters-Arts, M., Grossniklaus, U. & Angenent, G. C. The MADS
780 domain protein DIANA acts together with AGAMOUS-LIKE80 to specify the central
781 cell in Arabidopsis ovules. *Plant Cell* **20**, 2088-2101, doi:tpc.108.058958 (2008).

- 782 38 Steffen, J. G., Kang, I.-H., Portereiko, M. F., Lloyd, A. & Drews, G. N. AGL61
783 Interacts with AGL80 and Is Required for Central Cell Development in Arabidopsis.
784 *Plant Physiology* **148**, 259-268 (2008).
- 785 39 Pelaz, S., Gustafson-Brown, C., Kohalmi, S. E., Crosby, W. L. & Yanofsky, M. F.
786 APETALA1 and SEPALLATA3 interact to promote flower development. *Plant J* **26**,
787 385-394 (2001).
- 788 40 Kaufmann, K. *et al.* Target genes of the MADS transcription factor SEPALLATA3:
789 integration of developmental and hormonal pathways in the Arabidopsis flower. *PLoS*
790 *Biol* **7**, e1000090, doi:08-PLBI-RA-4384 (2009).
- 791 41 O'Maoileidigh, D. S. *et al.* Control of reproductive floral organ identity specification
792 in Arabidopsis by the C function regulator AGAMOUS. *Plant Cell* **25**, 2482-2503,
793 doi:10.1105/tpc.113.113209 (2013).
- 794 42 Mizukami, Y., Huang, H., Tudor, M., Hu, Y. & Ma, H. Functional domains of the
795 floral regulator AGAMOUS: characterization of the DNA binding domain and
796 analysis of dominant negative mutations. *Plant Cell* **8**, 831-845,
797 doi:10.1105/tpc.8.5.831 (1996).
- 798 43 Riechmann, J. L., Wang, M. & Meyerowitz, E. M. DNA-binding properties of
799 Arabidopsis MADS domain homeotic proteins APETALA1, APETALA3,
800 PISTILLATA and AGAMOUS. *Nucleic Acids Res* **24**, 3134-3141, doi:6t0273 [pii]
801 (1996).
- 802 44 Smaczniak, C., Muino, J. M., Chen, D., Angenent, G. C. & Kaufmann, K. Differences
803 in DNA Binding Specificity of Floral Homeotic Protein Complexes Predict Organ-
804 Specific Target Genes. *Plant Cell* **29**, 1822-1835, doi:10.1105/tpc.17.00145 (2017).
- 805 45 Guo, Y., Tian, K., Zeng, H., Gifford, D.K. A novel k-mer set memory (KSM) motif
806 representation improves regulatory variant prediction. *Genome Res* **28**, 891-900,
807 doi:10.1101/gr.226852.117 (2018).
- 808 46 Bowman, J. L., Alvarez, J., Weigel, D., Meyerowitz, E.M., Smyth, D.R. Control of
809 Flower development in Arabidopsis thaliana by APETALA1 and interacting genes.
810 *Development* **119**, 721-743 (1993).
- 811 47 Irish, V. F. & Sussex, I. M. Function of the apetala-1 gene during Arabidopsis floral
812 development. *Plant Cell* **2**, 741-753, doi:10.1105/tpc.2.8.741 (1990).
- 813 48 Masiero, S. *et al.* Ternary complex formation between MADS-box transcription
814 factors and the histone fold protein NF-YB. *J Biol Chem* **277**, 26429-26435,
815 doi:10.1074/jbc.M202546200 (2002).
- 816 49 Mendes, M. A. *et al.* MADS domain transcription factors mediate short-range DNA
817 looping that is essential for target gene expression in Arabidopsis. *Plant Cell* **25**,
818 2560-2572, doi:10.1105/tpc.112.108688 (2013).
- 819 50 Melzer, R., Verelst, W. & Theissen, G. The class E floral homeotic protein
820 SEPALLATA3 is sufficient to loop DNA in 'floral quartet'-like complexes in vitro.
821 *Nucleic Acids Res* **37**, 144-157, doi:10.1093/nar/gkn900 (2009).
- 822 51 Davies, B., Sommer, H., Schwarz-Sommer, Z. *Flower Development: Genetic Views*
823 *and Molecular News*. 167-184 (Springer Science and Business Media, 1999).
- 824 52 Brambilla, V. *et al.* Genetic and molecular interactions between BELL1 and MADS
825 box factors support ovule development in Arabidopsis. *Plant Cell* **19**, 2544-2556,
826 doi:10.1105/tpc.107.051797 (2007).
- 827 53 Liu, C., Xi, W., Shen, L., Tan, C. & Yu, H. Regulation of floral patterning by
828 flowering time genes. *Developmental cell* **16**, 711-722,
829 doi:10.1016/j.devcel.2009.03.011 (2009).

830 54 Vandenbussche, M., Theissen, G., Van de Peer, Y. & Gerats, T. Structural
831 diversification and neo-functionalization during floral MADS-box gene evolution by
832 C-terminal frameshift mutations. *Nucleic Acids Res* **31**, 4401-4409 (2003).

833 55 Egea-Cortines, M., Saedler, H. & Sommer, H. Ternary complex formation between
834 the MADS-box proteins SQUAMOSA, DEFICIENS and GLOBOSA is involved in
835 the control of floral architecture in *Antirrhinum majus*. *EMBO J* **18**, 5370-5379,
836 doi:10.1093/emboj/18.19.5370 (1999).

837 56 Gabadinho, J. *et al.* MxCuBE: a synchrotron beamline control environment
838 customized for macromolecular crystallography experiments. *J Synchrotron Radiat*
839 **17**, 700-707, doi:10.1107/S0909049510020005 (2010).

840 57 Kabsch, W. Integration, scaling, space-group assignment and post-refinement. *Acta*
841 *Crystallogr D Biol Crystallogr* **66**, 133-144, doi:10.1107/S0907444909047374 (2010).

842 58 de Folter, S. a. I., R.G.H. in *Plant Transcription Factors. Methods in Molecular*
843 *Biology (Methods and Protocols)* Vol. 754 (ed L. Yuan., Perry, S.) 145-165 (Humana
844 Press, 2011).

845 59 Gaspar, J. M. NGmerge: merging paired-end reads via novel empirically-derived
846 models of sequencing errors. *BMC Bioinformatics* **19**, 536, doi:10.1186/s12859-018-
847 2579-2 (2018).

848 60 Langmead, B. & Salzberg, S. L. Fast gapped-read alignment with Bowtie 2. *Nat*
849 *Methods* **9**, 357-359, doi:10.1038/nmeth.1923 (2012).

850 61 Li, H., Handsaker, B., Wysoker, A., Fennell, T., Ruan, J., Homer, N., Marth, G.,
851 Abecasis, G., Durbin, R., 1000 Genome Project Data Processing Subgroup. The
852 Sequence Alignment/Map format and SAMtools. *Bioinformatics* **25**, 2078-2079,
853 doi:10.1093/bioinformatics/btp352 (2009).

854 62 Zhang, Y. *et al.* Model-based analysis of ChIP-Seq (MACS). *Genome Biol* **9**, R137,
855 doi:10.1186/gb-2008-9-9-r137 (2008).

856 63 Jalili, V., Matteucci, M., Masseroli, M. & Morelli, M. J. Using combined evidence
857 from replicates to evaluate ChIP-seq peaks. *Bioinformatics* **31**, 2761-2769,
858 doi:10.1093/bioinformatics/btv293 (2015).

859 64 Freese, N. H., Norris, D. C. & Loraine, A. E. Integrated genome browser: visual
860 analytics platform for genomics. *Bioinformatics* **32**, 2089-2095,
861 doi:10.1093/bioinformatics/btw069 (2016).

862 65 Wickham, H. *ggplot2: Elegant Graphics for Data Analysis*. (Springer-Verlag 2016).

863 66 Bailey, T. L. *et al.* MEME SUITE: tools for motif discovery and searching. *Nucleic*
864 *Acids Res* **37**, W202-208, doi:10.1093/nar/gkp335 (2009).

865 67 Mathelier, A. & Wasserman, W. W. The next generation of transcription factor
866 binding site prediction. *PLoS Comput Biol* **9**, e1003214,
867 doi:10.1371/journal.pcbi.1003214 (2013).

868 68 Stigliani, A. *et al.* Capturing Auxin Response Factors Syntax Using DNA Binding
869 Models. *Mol Plant* **12**, 822-832, doi:10.1016/j.molp.2018.09.010 (2019).

870 69 Curtis, M. D. G., U. A Gateway Cloning Vector Set for High-throughput Functional
871 Analysis of Genes in *Planta*. *Plant Physiol* **133**, 462-469 (2003).

872 70 Benschmih, S. *et al.* Analysis of an activated ABI5 allele using a new selection
873 method for transgenic *Arabidopsis* seeds. *FEBS Lett* **561**, 127-131,
874 doi:10.1016/S0014-5793(04)00148-6 (2004).

875 71 O'Maoileidigh, D. S., Thomson, B., Raganelli, A., Wuest, S.E., Ryan, P.T.,
876 Kwasniewska, K., Carles, C.C., Graciet, E., Wellmer, F. Gene network analysis of
877 *Arabidopsis thaliana* flower development through dynamic gene perturbations. *The*
878 *Plant Journal* **83**, 344-358 (2015).

879 72 Clough, S. J. & Bent, A. F. Floral dip: a simplified method for *Agrobacterium*-
880 mediated transformation of *Arabidopsis thaliana*. *Plant J* **16**, 735-743 (1998).
881
882

Figures

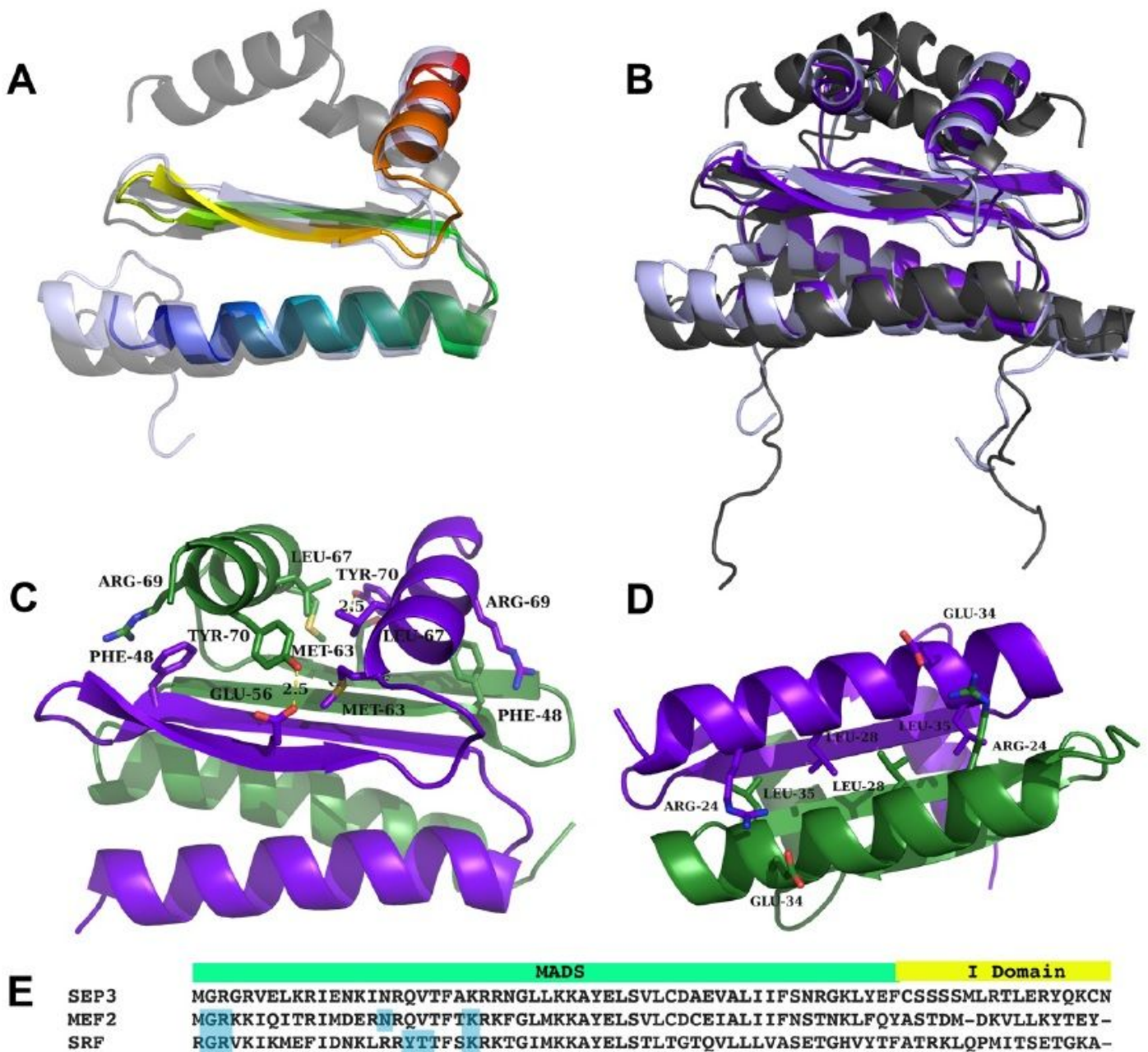


Figure 1

Structure and sequence of the SEP3 MI domain and corresponding SRF and MEF2 regions. (A) Overlay of SEP3 dimer (rainbow) and SRF (1HBX) dimer (gray). The I region is alpha helical for both structures, however the contacts with the M domain differ. (B) Overlay of SEP3 (dark purple) and MEF2A (3KOV, light purple) and SRF (gray) demonstrating the different conformations of the I region in the type II (MEF2-like) and I (SRF-like) MADS TFs. (C) SEP3 dimer with one monomer in purple and one in green. Amino acids important for interactions between I domains and between M and I domains are labelled and drawn as sticks. Hydrogen bonds are shown as dashed yellow lines. (D) View of the I domain with intermolecular

interactions from the N-terminal alpha helices shown. (E) Partial sequence alignment of SEP3 (accession NP564214.2), MEF2 (accession AAB25838.1) and SRF (accession P11831) corresponding to the region in the crystal structure. Residues directly contacting the DNA for MEF2 and SRF are highlighted in blue.

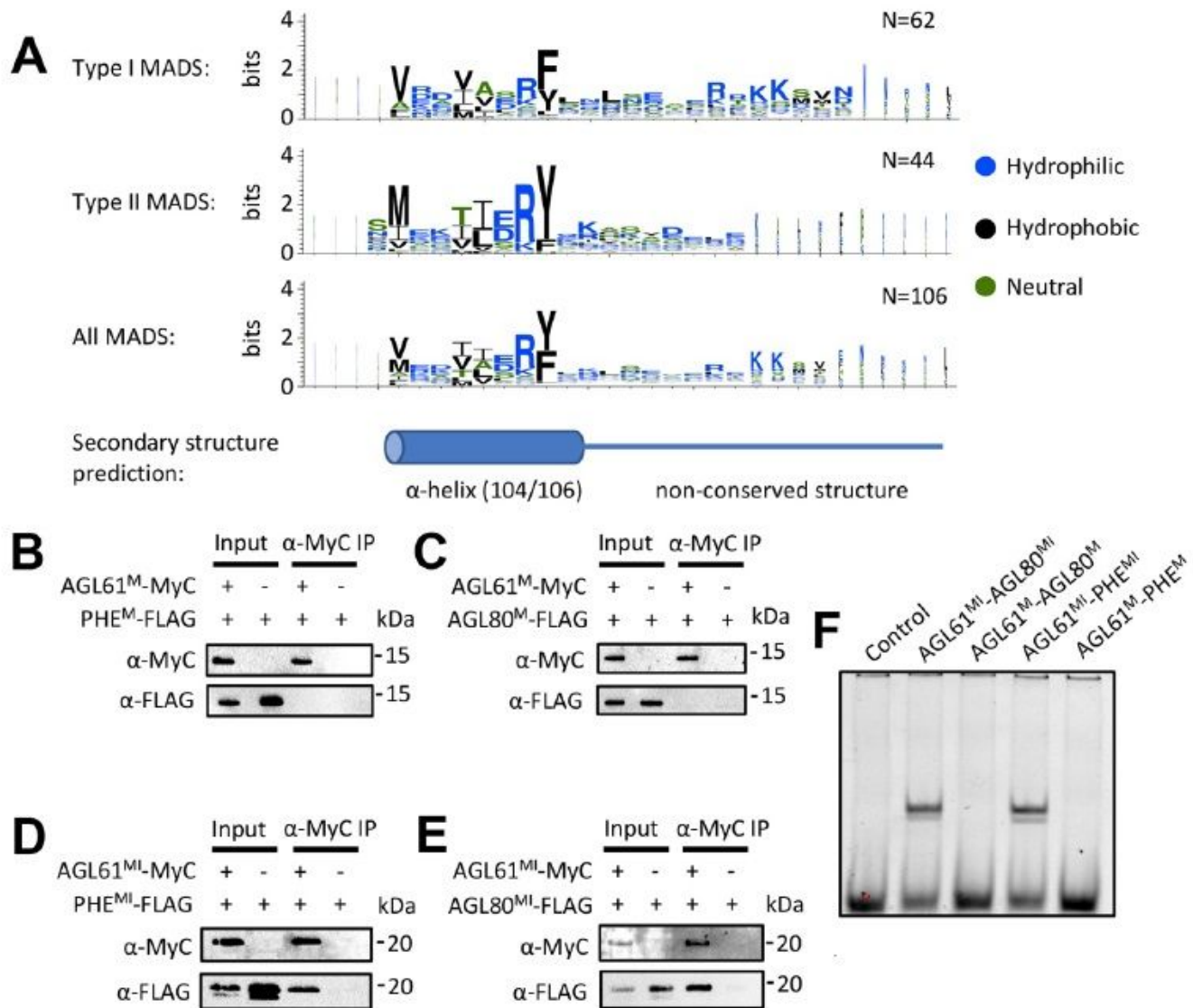


Figure 2

Type I MADS possesses I domain like region which is required for both dimerization and DNA binding. (A) Amino acid enrichment of the I region (~30 amino acids C-terminal to the M domain) of type I, type II and all MADS TFs, logos generated with WebLogo36. The overall height of the stack in each position indicates the sequence information content at that position, while the height of the amino acid symbols within the stack indicates the relative frequency at each position. The MADS TF sequences are taken from The Arabidopsis Information Resource (www.arabidopsis.org). (B-C) Pulldown assay showing that M domain of AGL61 (AGL61M) does not interact with the M domain of PHE (PHEM) or AGL80 (AGL80M). (D-E) Pulldown assay showing that the M domain plus the I like region of AGL61 (AGL61MI) interacts with the MI region of PHE (PHEMI) and AGL80 (AGL80MI). (F) EMSA assay showing that heterodimers

AGL61MI-AGL80MI and AGL61MI-PHEMI shift a DNA sequence containing a canonical CARG-box binding site from the SEP3 promoter, while their corresponding constructs without the I region do not exhibit any binding.

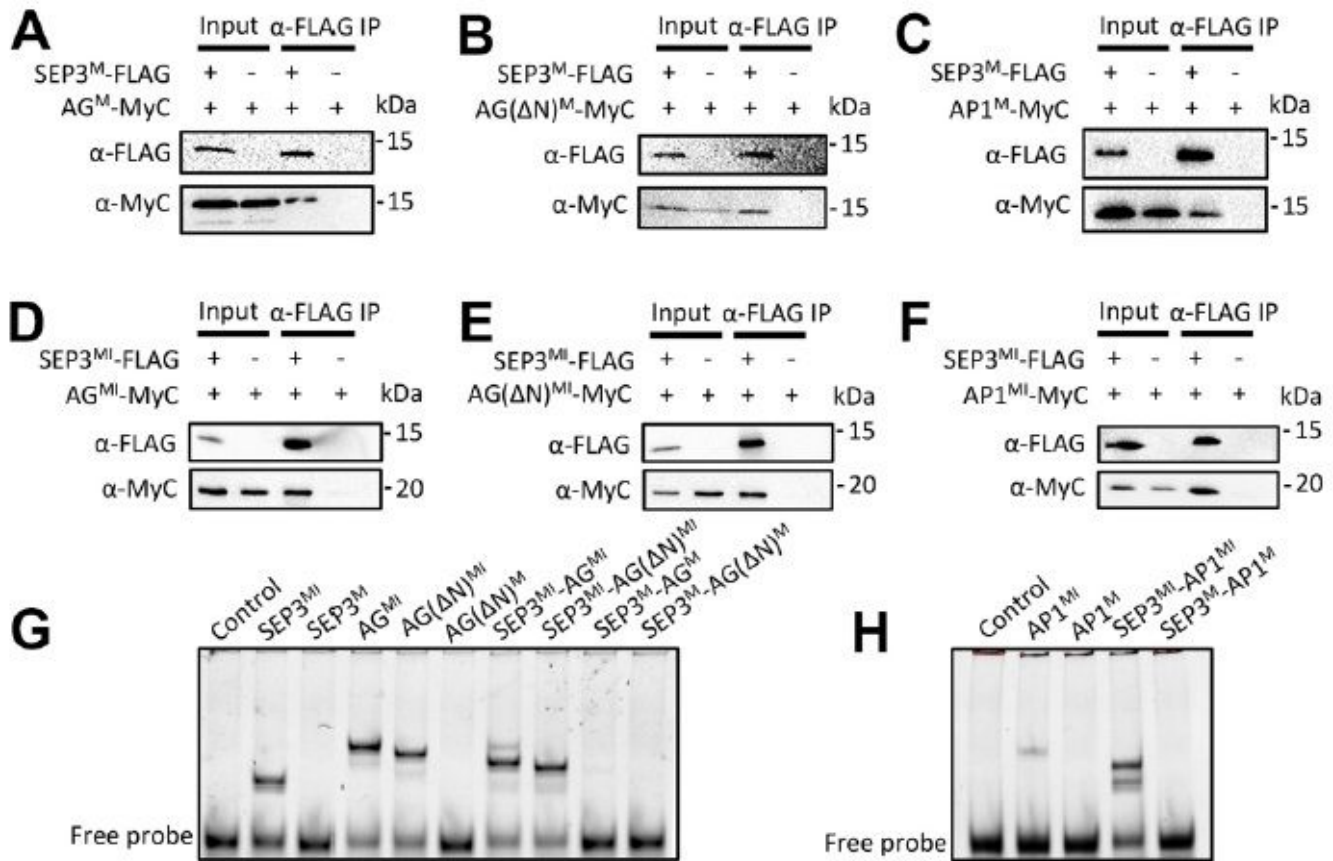


Figure 3

Type II MADS TFs require the I domain for DNA binding but not dimerization. (A-C) Pull-down assay showing that the M domain of SEP3 (SEP3M) interacts with the M domains of AG (AGM), AG with the first 16 N-terminal amino acids deleted (AG(ΔN)M) and AP1 (AP1M), respectively. (D-F) Pull-down assay showing that the MI domain of SEP3 (SEP3MI) interacts with the MI domain of AGMI, AG(ΔN)MI and AP1MI, respectively. (G and H) EMSA assay showing that homodimers from SEP3MI, AGMI, AG(ΔN)MI and AP1MI, and heterodimers SEP3MI-AGMI, SEP3MI-AG(ΔN)MI and SEP3MI AP1MI shift a DNA sequence containing a canonical CARG-box binding site (as per Figure 2), while their corresponding constructs without the I domain can not, suggesting that the I domain in type II MADS TFs is required for DNA binding.

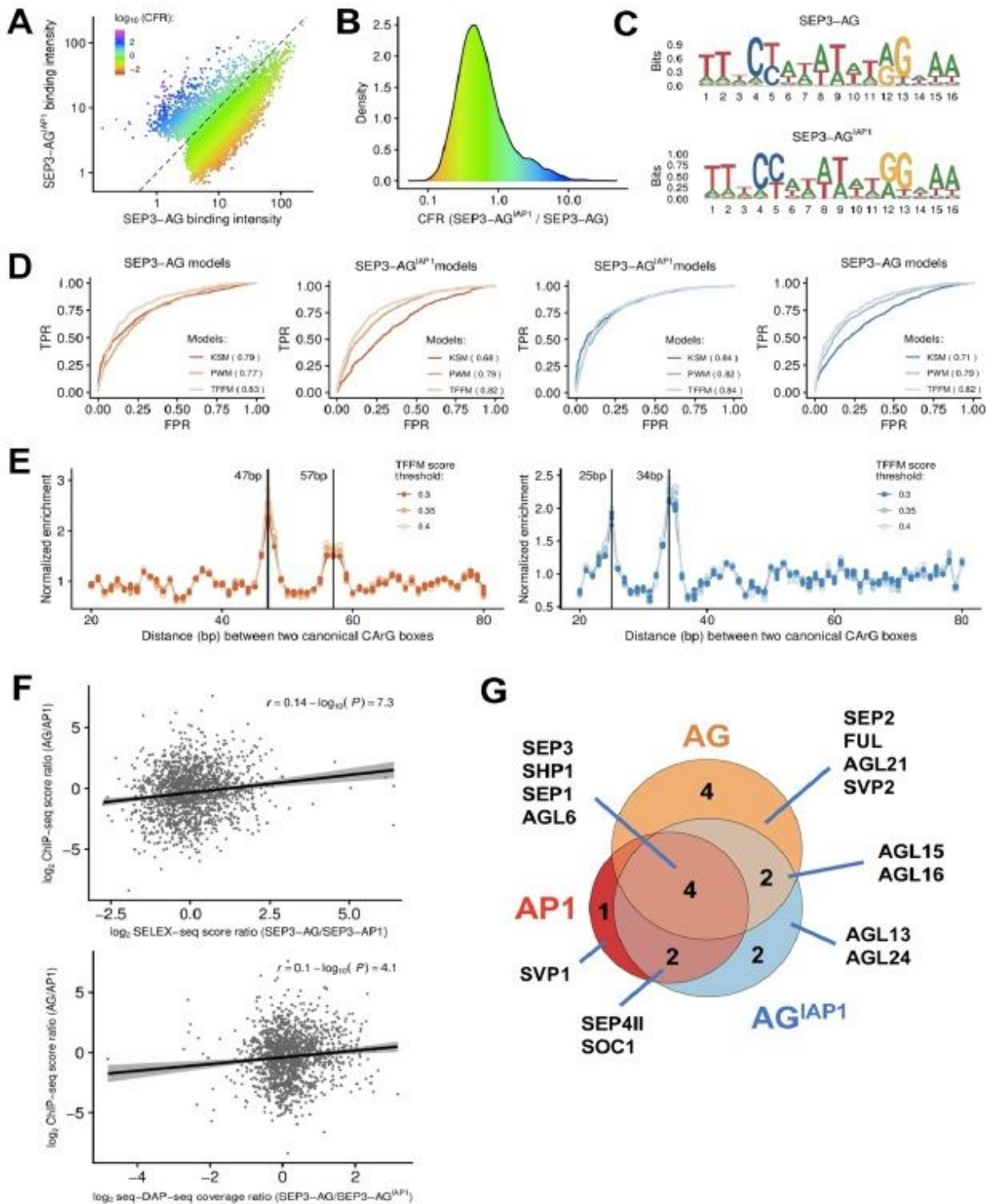


Figure 4

DNA-binding and protein interactions patterns. (A) Comparison of SEP3-AG and SEP3-AGIAP1 seq-DAP-seq binding intensity (\log_{10} of reads per kb per million of reads mapped in bound regions) and color-coded by purple-blue (SEP3-AGIAP1-specific) to orange-red (SEP3-AG-specific) according to \log_{10} of SEP3-AGIAP1/SEP3-AG. (B) Density plot showing data as per A. (C) Logos derived from PWM-based models obtained for SEP3-AG and SEP3-AGIAP1. (D) Predictive power of TFBS models. Models are built

using 600 sequences best bound by each of the two heterocomplexes and are searched against 1,073 SEP3-AG (orange) and 1,073 SEP3-AGIAP1 (blue) specific regions, defined as the top 15% of sequences that are most strongly bound by one complex relative to the other. Matrix-based models (PWM and TFFM) are not able to differentiate SEP3-AG and SEP3-AGIAP1 binding whereas k-mer-based analysis is able to better predict binding for the respective datasets. (E) SEP3-AG favors intersite spacings of 47 and 57 bp based on SEP3-AG specific regions. SEP3-AGIAP1 favors intersite spacings of 25 and 34 bp based on SEP3-AGIAP1I specific regions. (F) Top, published SELEXseq for SEP3-AP1 and SEP3-AG 5 comparing the normalized score ratios (SEP3-AG/SEP3-AP1) for SELEX-seq and score ratios (AG/AP1) ChIP-seq at 1,500 SEP3 best bound loci in ChIP-seq show a positive correlation, suggesting that SEP3- AP1 and SEP-AG bind different sequences in vivo and that in vitro binding is able to differentiate bound sequences that are more SEP3-AP1-like versus SEP3-AG-like. Bottom, SEP3-AG and SEP3-AGIAP1I seq-DAP-seq coverage as per SELEXseq scores. A positive correlation is observed suggesting that, in vitro, the swap of AP1 I domain in AG is able to recover some of the binding specificity of SEP3-AP1. (G) Yeast two-hybrid assays using AG, AP1 and AGIAP1 as bait against MIKCC MADS TFs in Arabidopsis. Data shows that AGIAP1 loses AG interactors and gains AP1 interactors.

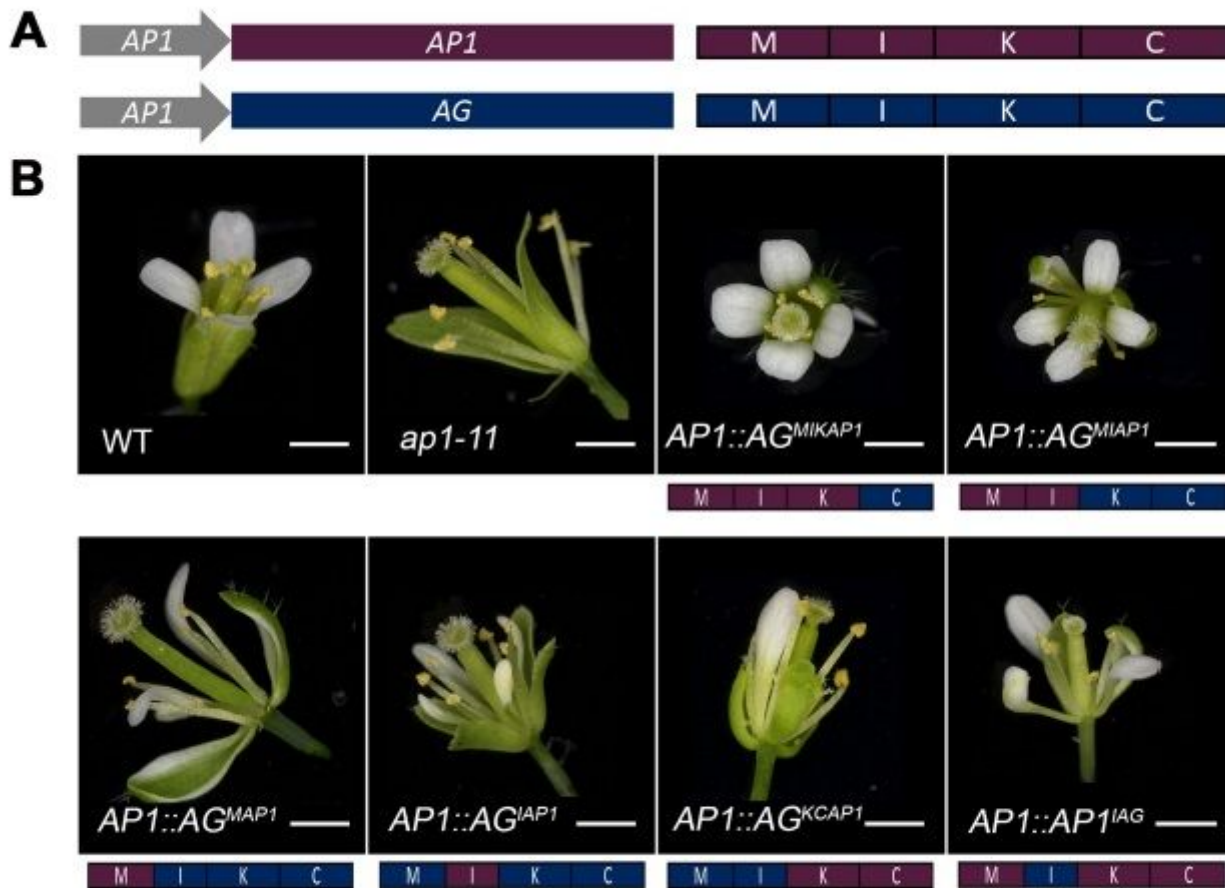


Figure 5

Primary transformants in the *ap1* mutant background exhibit a spectrum of complementation. (A) Schematic of the constructs and proteins produced with AP1 protein in purple and AG in dark blue. Domains are labeled MIKC. (B) Flower phenotypes of T1 transformants ($n \geq 10$). All transformants were in the *ap1-11* background. Phenotypes for WT and *ap1-11* are shown. The domains corresponding to AP1 and AG are colored as per (A) and shown schematically below each panel.

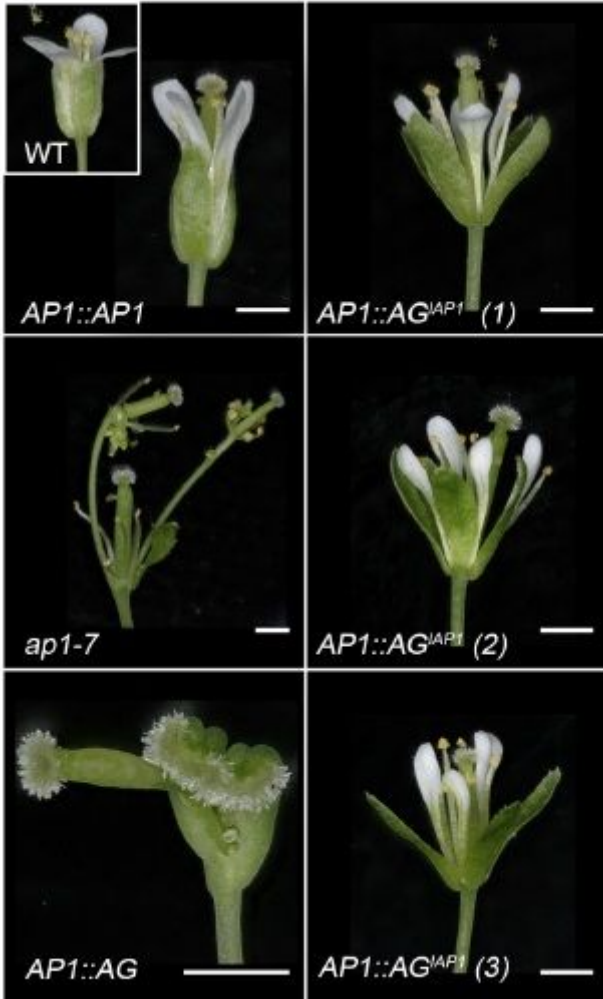


Figure 6

AP1:AGIAP1 expression largely complements the *ap1-7* flower phenotype. *ap1-7* lines expressing either AP1 (AP1::AP1), AG (AP1::AG) or AGIAP1 (AP1::AGIAP1) under the control of the AP1 promoter were grown at 22 °C in long days. A typical WT flower is shown as an insert in the upper left panel. Representative flowers for 3 independent AP1::AGIAP1 lines are presented and one representative flower from AP1::AG and AP1::AP1 expressing lines. While the first whorl in *ap1-7* is replaced by bract or stipule with axillary buds and petals are missing in the second whorl, AP1::AGIAP1 expression restores WT first and second whorl organs, while AG expression triggers carpel development in the first whorl and absence of petals in the second whorl. Scales bars = 1 mm.

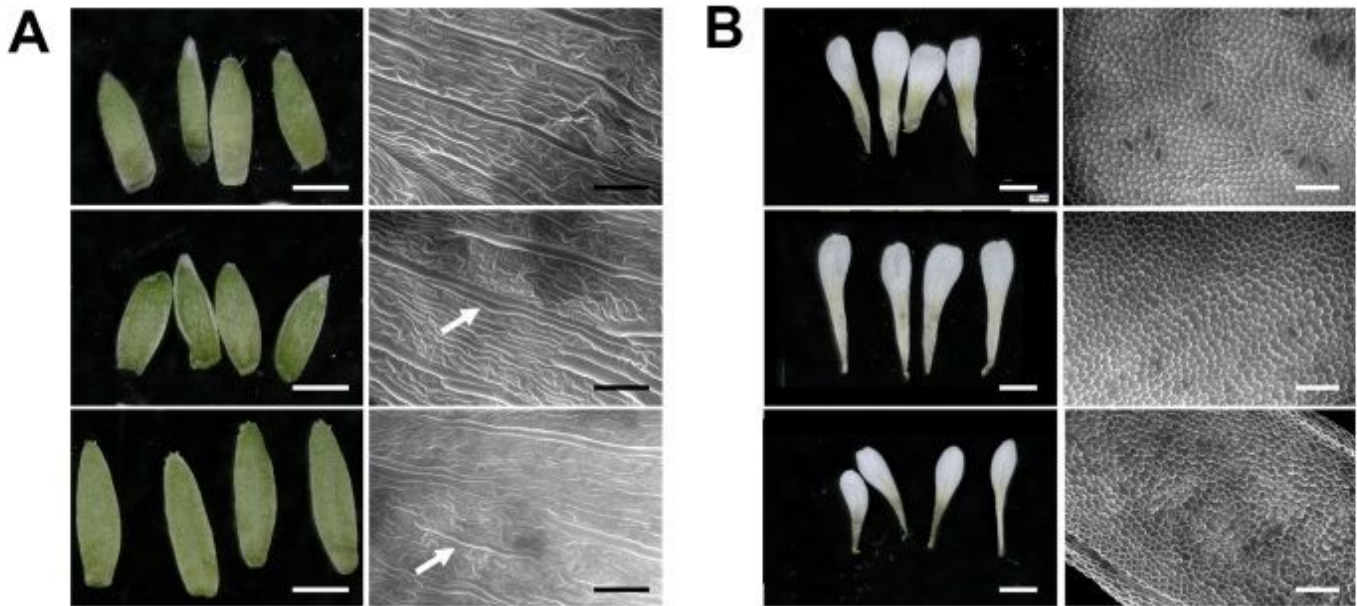


Figure 7

First and second whorls cell identity are complemented in *ap1-7* plants expressing AGIAP1. First (A) and second (B) whorl organs were removed from WT, and flowers from AP1 or AGIAP1 expressing *ap1-7* plants. First whorl organs in AGIAP1 expressing plants are slightly longer compared to WT and AP1 expressing plants (A, left panel). Second whorl organs in AGIAP1 expressing plants are slightly smaller compared to WT and AP1 expressing plants (B, left panel). Epidermal cell identity, observed by SEM, show characteristic WT elongated sepal cells in AP1 and AGIAP1 expressing plants (A, right panel) and characteristic WT conical cells in petals from AP1 and AGIAP1 expressing plants (B, right panel). A small number of epidermal cells typical of leaves are also seen in AGIAP1 expressing plants and to a lesser extent in AP1 expressing plants (arrow). Scale bars indicate 100 μ M for SEM images and 1 mm for organ photographs.

Supplementary Files

This is a list of supplementary files associated with this preprint. Click to download.

- [Supplementarysubmissioncompressed.pdf](#)